

Article

ZnFe₂O₄/Zeolite Nanocomposites for Sorption Extraction of Cu²⁺ from Aqueous Medium

Elena Tomina^{1,2}, Lyudmila Novikova^{1,*} , Alexandra Kotova¹, Anna Meshcheryakova², Victoria Krupskaya^{3,4} , Ivan Morozov³ , Tatiana Koroleva^{3,4}, Ekaterina Tyupina^{5,6} , Nikolai Perov⁷  and Yuliya Alekhina⁷

- ¹ Department of Chemistry, Voronezh State University of Forestry and Technologies Named after G.F. Morozov, 8 Timiryazeva Str., Voronezh 394087, Russia; tomina-e-v@yandex.ru (E.T.); sura.kotova22@list.ru (A.K.)
- ² Department of Materials Science and Nanosystems Industry, Voronezh State University, 1 Universitetskaya pl., Voronezh 396036, Russia; anna-meshcheryakova@internet.ru
- ³ Institute of Geology of Ore Deposits, Petrography, Mineralogy and Biochemistry RAS, 35, Staromonetny Per., Moscow 119017, Russia; krupskaya@ruclay.com (V.K.); ivan.morozov@yandex.ru (I.M.); tanakoro@yandex.ru (T.K.)
- ⁴ Faculty of Geology, Department of Engineering and Environmental Geology, Lomonosov Moscow State University, GSP-1, Leninskie Gory, Moscow 119991, Russia
- ⁵ Department of High Energy Chemistry and Radioecology, Mendeleev University of Chemical Technology of Russia, 9, Miusskaya Square, Moscow 125047, Russia; tk1972@mail.ru
- ⁶ Department of Closed Nuclear Fuel Cycle Technology, National Research Nuclear University «MEPhI», Kashirskoe Highway 31, Moscow 115409, Russia
- ⁷ Faculty of Physics, Department of Magnetism, Lomonosov Moscow State University, GSP-1, Leninskie Gory, Moscow 119991, Russia; perov@magn.ru (N.P.); ya.alekhina@physics.msu.ru (Y.A.)
- * Correspondence: yonk@mail.ru; Tel.: +7-(473)-2537-659

Abstract: In order to enhance the efficiency of heavy metal ion extraction from aqueous medium, new nanocomposite magnetic sorbents were synthesized on the base of natural zeolite (Zt) and nanoparticles of ZnFe₂O₄ (F). The composition, structure and physical–chemical properties of new composites with 2% (Zt-2F), 8% (Zt-8F) and 16% (Zt-16F) of zinc ferrite were characterized by XRD, BET adsorption–desorption of nitrogen, SEM with elemental mapping, TEM and magnetometry. The sorption capacity of materials was assessed towards Cu²⁺ ions in aqueous solutions, for which kinetic and equilibrium features of sorption were established. The maximal sorption capacity (a_{max}, mg/g) of the studied materials increased in the order: Zt (19.4) < Zt-2F (27.3) < Zt-8F (30.2) < Zt-16F (32.8) < ZnFe₂O₄ (161.3). The kinetics of the sorption process followed a pseudo-second order kinetic model. The sorption equilibrium at zinc ferrite was successfully described by the Langmuir model, while the Freundlich model better fitted the sorption equilibrium on zeolite and composites. The efficiency of Cu²⁺ ion extraction from 320 mg/dm³ aqueous solution was 63% for composite Zt-16F and 100% for a sample of ZnFe₂O₄. It was established that the proposed composite sorbents provide the operation of several cycles without regeneration, they can be easily recycled with 0.1 N HCl solution and are capable of magnetic separation. The advantages of new composites and the proposed method of synthesis allow recommending these materials as effective sorbents of heavy metals from wastewater.

Keywords: zinc ferrite; nanoparticles; clinoptilolite; nanocomposite; sorption; copper ions; kinetics; equilibrium; water treatment; magnetic separation



Citation: Tomina, E.; Novikova, L.; Kotova, A.; Meshcheryakova, A.; Krupskaya, V.; Morozov, I.; Koroleva, T.; Tyupina, E.; Perov, N.; Alekhina, Y. ZnFe₂O₄/Zeolite Nanocomposites for Sorption Extraction of Cu²⁺ from Aqueous Medium. *AppliedChem* **2023**, *3*, 452–476. <https://doi.org/10.3390/appliedchem3040029>

Received: 16 August 2023

Revised: 15 September 2023

Accepted: 26 September 2023

Published: 30 September 2023



Copyright: © 2023 by the authors. Licensee MDPI, Basel, Switzerland. This article is an open access article distributed under the terms and conditions of the Creative Commons Attribution (CC BY) license (<https://creativecommons.org/licenses/by/4.0/>).

1. Introduction

Adsorption technology is the most widespread, universal and, therefore, highly demanded technology in industry and laboratory practice for the separation of substances and mixtures, isolation of individual components and purification of industrial blends and wastewaters [1–4]. The main goals for the development and application of the sorption method are related to increasing the sorbents' selectivity and the efficiency of the

components' extraction, reducing the cost of production, possibilities of regeneration and ways of sorbents disposal, and overall economic efficiency of the sorption process as a whole. At the present stage of scientific and technological development, these problems can be solved by increasing the involvement of renewable resources (such as natural organic and inorganic materials, man-made materials, industrial waste, etc.) to create new sorption-active materials and improve waste-free production technologies [5–8]. As a trend, the novel materials being created are composite and/or hybrid materials, both organo-inorganic and inorganic-organic [9,10], which acquire new functionality during synthesis. In this trend, it is possible to combine such properties as a developed surface and porosity with outstanding physical and chemical activity, sorption and catalytic ability, electrical and magnetic properties, biological activity, strength characteristics, stability in various media, etc. [4,11–13].

In recent years, much attention has been paid to nanosized ferrites with a spinel structure as possible magnetically controllable sorbents. Nanosized cobalt ferrite CoFe_2O_4 proved to be an effective adsorbent of chromium (III) and cadmium (II) ions [14], phosphate anions [15], arsenic [16], lead, zinc and a number of organic dyes (Congo red, malachite green, eriochrome black, etc.) [17–19]. The maximal removal efficiencies for Pb^{2+} (96%) and Zn^{2+} (92%) ions, as well as for Congo red (99%) and malachite green (92.5%) was reached in [20] by applying the nanosized CoFe_2O_4 as a sorbent. Similar behavior was found in [21] for nanoparticles of mixed cobalt–zinc ferrites $\text{Co}_x\text{Zn}_{1-x}\text{Fe}_2\text{O}_4$ having a high sorption capacity for lead ions, in which the content of zinc determined the magnetocrystalline anisotropy and the superparamagnetic/ferromagnetic state of the particles. Nanoparticles of manganese ferrite, MnFe_2O_4 , synthesized from low-grade manganese ore [22], proved to be effective for the purification and recovery of strategically important tungsten, molybdenum and rhenium from wastewater.

The use of various synthesis routes (hydrothermal, solvothermal, co-precipitation, sol-gel, template, and electrospinning, etc.) makes it possible to form spinel-ferrite nanoparticles with a variable size, porosity and morphology, and to successfully control their physicochemical characteristics [23–27]. In addition, recently it became possible to synthesize ferrites from industrial wastes [28,29], which puts them into the category of renewable resources. This, in turn, makes it possible to transfer, without restrictions, from purely chemical laboratory synthesis methods to large-scale production of metal ferrites.

Among all metal ferrites, zinc ferrite should be noted especially for its extremely high chemical stability, magnetic properties, non-toxicity for living organisms and environmental safety [24,29,30]. Materials based on zinc ferrite possess photocatalytic activity and activity in Fenton reactions that allows using them as photoadsorbents and photocatalysts for the treatment of various media and degradation of organic pollutants [12,30–32]. In addition, recent studies indicated a noticeable adsorption capacity of nanomaterials based on ZnFe_2O_4 , with respect to selenium ions (43.67 mg/g at pH 2.5) [28] and heavy metal ions (49.42, 54.69 and 12.34 mg/g for Ni^{2+} , Cd^{2+} and Cr^{3+} [23,33]) from the aquatic environment, which is important for solving the problem of wastewater treatment and converting industrial waste into valuable materials for recycling.

To overcome the problem of agglomeration of nanoparticles and enhance the sorption and catalytic characteristics of materials, it is applied by introducing the nanoparticles of spinel-ferrites into polymer gels or into a composition of composites on the base of various matrixes. Thus, stable $\text{PVP@MnFe}_2\text{O}_4$ nanoparticles with a high affinity for heavy metal ions (Pb^{2+} , Cd^{2+} , Ni^{2+}) were obtained in [34] by decorating manganese ferrite with polyvinylpyrrolidone. In [35], CuFe_2O_4 particles were immobilized on the surface of chitosan, and an effective adsorbent $\text{CuFe}_2\text{O}_4\text{@Chitosan}$ and a catalyst for the decomposition of antibiotics in an aqueous medium were obtained. The presence of ZnFe_2O_4 [36], MnFe_2O_4 [37,38] and CoFe_2O_4 [39] nanoparticles in the composition of nanocomposites with mineral matrixes (aluminosilicates, hydroxyapatite) caused a strong catalytic effect in Fenton redox reactions, the photocatalytic degradation of organic pollutants and, moreover, suppressed the growth of pathogenic microorganisms *Staphylococcus aureus*, *Bacillus*

subtilis, *Pseudomonas aeruginosa* and *Escherichia coli* [37]. Nanocomposites based on a carbon matrix (CNT, graphene oxide) and metal ferrites efficiently adsorb a wide range of organic pollutants [40–43]. Sorption on such composites occurs due to both π - π interaction between hexagonally arranged sp^2 hybridized carbon atoms of CNTs and the aromatic backbone of dyes, and due to electrostatic interaction or hydrogen bonding between functional groups of the sorbate molecule and CNT surface, thus contributing to their active photocatalytic degradation.

For the applications of sorption processes to wastewater treatment, we consider it promising to use composite materials based on a less expensive dispersion matrix, in which the magnetic component of nanosized ferrite makes it possible to obtain a magnetically controllable sorbent. Composite materials that combine a sorbent-carrier and a ferrite spinel with magnetic properties can be selectively and efficiently isolated from aqueous solutions using an external magnetic field. In our opinion, the most promising materials for the synthesis of composites with the participation of nanosized spinel ferrites and their application for industrial wastewater treatment are natural mineral sorbents: clays, flasks, zeolites, zeolite-containing rocks, etc. The advantage of such materials is, first of all, their natural origin, low cost, availability of extraction and processing, and substantial reserves [44–46]. Already in the natural state, aluminosilicates exhibit a noticeable ion-exchange and sorption capacity, and catalytic and molecular sieve properties [47–49]. Furthermore, using various types of chemical [50,51], physical [52–54] and mechanical [55,56] modifications, a purposeful transformation of the structure, composition and physicochemical properties of aluminosilicates is carried out, creating new complex materials on their basis [37,47,57].

In recent years, water pollution with Cu (II) ions has become a serious environmental problem worldwide due to the growing discharge of copper-containing wastewater [58,59]. The main sources contributing to the appearance of copper in wastewater are galvanic production at machine-building and instrument-making enterprises, effluents from mining and processing, and mine water from the mining copper industry [60,61]. Despite the fact that copper is an essential element for the regulation of biological processes in all living organisms (metabolism, nerve function, hemoglobin synthesis and bone development), its excess above the permissible limits causes serious problems in the human body and living beings [62,63]. Copper compounds lead to dysfunction of the central nervous system, heart disease, anemia, liver damage and they have a carcinogenic effect; therefore, they are classified as environmentally hazardous compounds. Poisoning with a large amount of copper leads to Wilson's disease, where an excess of copper is deposited in the brain tissues, skin, liver and pancreas.

The purpose of this work was to produce and characterize new nanocomposite magnetically controllable sorbents based on natural zeolite and zinc ferrite nanoparticles, and to establish the patterns of sorption of copper ions from an aqueous medium by the proposed sorbents. For this, zinc ferrite nanoparticles were synthesized and introduced, in various amounts, into a composite material based on natural aluminosilicate. The composition, structure, and physicochemical and magnetic properties of the new composites were characterized. The sorption characteristics of the materials were determined in aqueous solutions containing copper ions. The possibility of regeneration of sorbents and their magnetic extraction was shown.

2. Materials and Methods

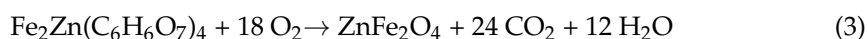
The objects of investigations included natural clinoptilolite-rich zeolite (Zeocem, Bystré, Slovakia), having particle size $\leq 50 \mu\text{m}$, and nano powder of zinc ferrite, synthesized by an acetate burning method, similar to that in [64].

2.1. Synthesis of ZnFe_2O_4 Nanoparticles

For the synthesis of ZnFe_2O_4 nanoparticles, stoichiometric amounts of reagents of analytical grade ($\text{Fe}(\text{NO}_3)_3$, $\text{Zn}(\text{NO}_3)_2$, 28% NH_4OH , 1 M citric acid) were used. At the first step, 27.64 g of iron (III) nitrate (chemically pure, KhCh TU 6-09-02-553-96, JSC LenReaktiv,

Saint Petersburg, Russia) and 10.16 g of zinc nitrate (chemically pure, HCh CAS 10196-18-66 LLC "Spectrum-Chem", Moscow, Russia) were dissolved in 100 cm³ of distilled water at ambient temperature under stirring for 5 min. Then, 10 cm³ of NH₄OH (analytical grade, GOST 3760-79, JSC LenReaktiv, Saint Petersburg, Russia) was added at pH ≈ 7 under stirring for the next 5 min. A brown precipitate of the mixture of zinc and iron hydroxides formed (Equation (1)). Then, 35 cm³ of the prepared 1 M citric acid solution (chemically pure, GOST 3652-69, JSC LenReaktiv, Saint Petersburg, Russia) was added to the reaction vessel and heated on a gas burner. Within 15 min there was a gradual dissolution of the precipitate due to the formation of soluble citrate (Equation (2)). Further heating of the mixture for the next 1.5 h caused water evaporation and self-ignition of the gel-like iron–zinc citrate formed. As a result of combustion, a powder of ZnFe₂O₄ formed (Equation (3)).

The chemical reactions occurred during the synthesis can be expressed by the following equations:



The precipitate obtained in the reaction (3) was washed with water, dried and finally calcined at 600 °C in the muffle furnace (SNOL 8.2/1100, AB Umega, Utena, Lithuania) for 1 h.

2.2. Synthesis of ZnFe₂O₄/Zeolite Composite Materials

For the synthesis of a series of ZnFe₂O₄/zeolite composites, samples with 2, 8 and 16 mass % of ZnFe₂O₄, the corresponding amounts of zeolite and zinc ferrite powder were taken to prepare 5 g of each composite sample. The precursors were mixed, adding 1 mL of ethanol dropwise and under continuous stirring for 10 min. The resulting paste was dried in the air at room temperature and annealed at 500 °C for 1 h. The fabricated samples of the composites were designated Zt-2F, Zt-8F and Zt-16F, which corresponded to the content of 2, 8 and 16 mass % of ZnFe₂O₄ nanopowder in the composite with zeolite (Zt).

2.3. Characterization Methods

The phase composition and the structure of the samples were determined from the XRD-spectra recorded on the Ultima-IV (Rigaku, Tokyo, Japan) diffractometer with Cu-Kα radiation, D/Tex-Ultra detector and the range of imaging angles 2θ = 3–65°.

The microimages of the samples of zeolite, zinc ferrite and composites were obtained on a JSM-IT500 scanning electron microscope (JEOL, Tokyo, Japan), and the particle size and shape were studied using transmission electron microscopy on a CarlZeiss LIBRA 120, JEM-1400 microscope. The quantitative chemical composition of the samples, as well as the elemental mapping of copper for samples of zinc ferrite and composites after Cu²⁺-sorption, were determined by local X-ray spectral microanalysis using a scanning electron microscope JSM-6380LV (JEOL, Tokyo, Japan) with an energy dispersive microanalysis system INCA 250 from "Oxford Instruments", Abingdon, UK (EDS analysis).

The specific surface area and porosity of materials were assessed from the experimental nitrogen sorption–desorption isotherms at –196 °C using a Quadra Sorb Quantachrome Instruments unit, Boynton Beach, FL, USA. Prior the measurement, a charge of the sample (150 mg) was outgassed at 100 °C for 4 h. The values of total pore volume and average pore diameter were calculated by the DFT method at the Quantachrome Quadra Win Software version 5.02.

2.4. Adsorption Experiments

Adsorption ability of the studied materials was determined in relation to Cu^{2+} -ions at the pH of model aqueous solutions of CuSO_4 under static conditions by the batch adsorption technique. The stock solutions of various concentrations were prepared from CuSO_4 (analytical grade, JSC LenReaktiv, Saint Petersburg, Russia) and distilled water. The pH of the solution was determined using a Yinkmik BLE-C600 instrument (Ji Nan Runjie Electronic Technology Co., Ltd., Shandong, China). The pH values of solutions are presented in Table S1 of Supplementary Materials.

For kinetic studies of adsorption, 200.0 mg of the sorbent was added into a flask with 20.0 cm^3 of 0.01 N CuSO_4 solution, and kept for 5, 10, 20, 40 and 60 min at 20 °C, periodically shaking. The sorption experiments were carried out for two parallel samples. Afterwards, the sorbent was filtered off and Cu^{2+} -concentration in the filtrate was determined by the photocolometric method [65–67] in the form of ammonia complexes. For this, 10 cm^3 of 5% NH_4OH was added to a 10 cm^3 aliquot of a solution containing Cu^{2+} ions, filled with distilled water until 25 cm^3 volume, and the resulting solution was photometrically measured using a spectrophotometer KFK-3-01-“ZOMZ” (JSC “ZOMZ”, Moscow, Russia) at $\lambda_{\text{max}} = 660 \text{ nm}$.

The kinetic curves were used to determine the time of adsorption equilibrium establishment, as well as they were processed by pseudo-first and pseudo-second order kinetic models [68,69]. To determine the most appropriate kinetic model, the mean squared error (RMSE) and the quadratic coefficient of multiple regression (R^2) were used as statistical criteria.

The equilibrium of sorption was characterized by studying the experimental isotherms of copper ion sorption by the investigated materials in the concentration range of 0.005–0.1 N CuSO_4 , at a sorbent–solution ratio of 1:100 and at $t = 20 \text{ }^\circ\text{C}$. To determine the adsorption value, 200.0 mg of the adsorbent was added to a flask with 20.0 cm^3 of a CuSO_4 solution of the appropriate concentration, periodically shaken, and kept for 30 min to reach equilibrium. The sorption was carried out for two parallel samples. Then, the sorbent was filtered off and the concentration of copper ions in the filtrate was determined by the photocolometric method. The results were statistically processed using a Student's *t*-test for the confidence level $\alpha = 0.95$.

The value of adsorption (a , mg/g) and the degree of water purification, R , %, were determined by the formulas:

$$a = \frac{(C_{\text{in}} - C_{\text{eq}}) * V * M_{\text{eqv}}}{m}, \quad (4)$$

$$R, \% = \frac{(C_{\text{in}} - C_{\text{in}})}{C_{\text{in}}} * 100\%, \quad (5)$$

where C_{in} and C_{eq} —initial and equilibrium solution concentration, mol-equiv/ dm^3 ; M_{eqv} —molar mass of equivalent, g-eq/mol; V —volume of solution, dm^3 ; and m —mass of sorbent, g.

The possibility of spent sorbent recycling was studied using 0.1 N NaCl, NaOH and HCl solutions for regeneration. A portion of the sorbent (200.0 mg) was placed in 20 cm^3 of an appropriate electrolyte solution, left for 30 min, filtered and the amount of desorbed copper (mg/g) was determined as $Q_{\text{des}} = C_{\text{eqv}} * V * M_{\text{eqv}} / m$.

The possibility of regeneration of the spent sorbents was studied using 0.1 N NaCl, NaOH and HCl solutions. In addition, in the absence of sorbent regeneration, the number of adsorption cycles of sorption from 0.01 N CuSO_4 solution was also determined.

2.5. Assessment of Magnetic Properties

Magnetic properties of the sorbents and their ability for magnetic separation were qualitatively studied using a neodymium magnet N42 (Shenzhen Wit Magnet Co., Ltd., Shenzhen, Guangdong, China) with a size of 30 × 10 mm (residual magnetic induction

1.30–1.33 T, coercive force 12 kOe). The magnet was brought to the flask with equilibrium solution and the sorbent and the ability of the suspension for separation was observed.

For quantitative characterization of magnetic properties, the magnetization curves of the samples were studied using a Lakeshore 7407VSM vibrating magnetometer (Lake Shore Cryotronics, Inc., Westerville, OH, USA) at room temperature in magnetic fields up to 16 kOe. The powders were sealed in polyethylene capsules and laminated, to prevent particle movement during measurements. The sample was fixed on the holder with a Teflon tape. The signal from the holder, capsules and fum-tape was subtracted from the signal to isolate the contribution of the samples. The results of magnetic measurements were processed using the “Origin” software package version 9.0.

3. Results and Discussion

3.1. Characterization of the Structure and Compositions of Zeolite, $ZnFe_2O_4$ and Composites on Their Base

According to X-ray diffraction analysis, the sample of zinc ferrite contains 99.0% of $ZnFe_2O_4$ ($d = 2.56, 2.12, 1.73, 1.63, 1.50 \text{ \AA}$, etc.) and 1.0% of hematite (2.71 \AA). The mineral composition of the zeolite sample was mainly represented by clinoptilolite with a series of reflections of $9.1, 8.0, 6.82, 3.98, 3.93, 2.99 \text{ \AA}$, etc., as well as clay minerals including smectite with a basal reflection (001) with interplanar distance $d = 12.0 \text{ \AA}$ and illite with a basal reflection of 10.1 \AA , in addition to on-clay minerals—quartz ($d = 4.25, 3.34, 2.46, 2.28, 2.13, 1.82, 1.54 \text{ \AA}$, etc.), cristobalite ($d = 4.04, 2.48 \text{ \AA}$, etc.), feldspars: albite and microcline ($d = 4.25, 3.36, 3.21 \text{ \AA}$, etc.) and opal (Figure 1).

The content of mineral phases in the zeolite sample was distributed as follows: clinoptilolite, 66.0%; smectite, 7.2%; illite, 6.6%; quartz, 1.7%; cristobalite, 5.0%; plagioclase (albite), 4.4%; potassium feldspar, 3.8%; and opal, 5.3%. The opal content was obtained by calculation after a full-profile XRD analysis of the diffraction pattern.

The diffraction patterns of composite samples are characterized by the presence of reflections of both used precursors with a clear tendency for raising the intensity of zinc ferrite bands with an increase in its content in the composite. At the same time, the main reflections of clinoptilolite did not change their position and intensity, which indicated the preservation of the zeolite structure in the course of composite manufacturing.

Figure 2 demonstrates the X-ray diffraction patterns of the zinc ferrite sample before and after copper sorption. A new phase with the crystal structure of the mineral brochantite ($d = 6.46, 5.39, 3.91, 3.20 \text{ \AA}$, etc.) appeared, apparently due to the presence of $CuSO_4$ from the equilibrium solution (aqueous solution of $CuSO_4$) in the sorbent phase after sorption. The crystal structure of zinc ferrite, as well as the structure of clinoptilolite, did not change after copper sorption.

According to Figure 3a, the synthesized sample of zinc ferrite was represented by uniform flattened particles with clearly distinguishable facets, mostly less than 60 nm in size, with a moderate agglomeration. Particles of 11–30 nm and 31–60 nm in size can be distinguished as the main fractions of particles (Figure 3b).

The data on the chemical composition of the samples determined from the EDS-analysis are summarized in Table 1. The value of the silicate modulus for the sample of natural zeolite equals $SiO_2/(Al_2O_3 + Fe_2O_3) = 6.06$; that is an attribute of a highly siliceous type. The primary exchangeable cations of zeolite are Ca^{2+} , K^+ and Mg^{2+} ions. The introduction of zinc ferrite nanoparticles into the composite led to a regular redistribution of its chemical composition in favor of an Fe_2O_3 and ZnO content increase.

Microphotographs of the samples of initial components were obtained in backscattered electrons, which allowed to distinguish ferrite particles in the composites.

The micrograph of zeolite sample without the addition of ferrite (Figure 4a) showed very large aggregates of zeolite crystallites. Due to the peculiarities of the crystal structure, it forms flattened prismatic crystals (lamellae) [70]. Lamellas of nanoscopic thickness (ca. 40 nm) have a length in the range of 300 nm–1 μm , and a width in the range of 300–700 nm. Such single crystals are connected face-to-face, forming dense aggregates, at the contact

points of which extended intergranular cracks (the largest mineral mesopores arise with a size of ca. 25–50 nm). Sometimes macropores (approx. 100 nm or 500 nm in size) can be present among the lamella blocks (Figure S1a).

The micrographs of the pure zinc ferrite sample (Figures 4d and S1d) clearly testified that it formed aggregates of lamellar crystallites. In a more detailed image of zinc ferrite in secondary electrons (Figure 5), one can see that large aggregates are composed of small flakes. Ferrite particles in the composites (Figure 4b,c) were clearly visible by their characteristic increased brightness, having evenly distributed in the zeolite phase. The change in the surface relief of resulting composites Zt-2F and Zt-16F (Figure S1b,c) was most likely caused by the filling of the interparticle macro- and mesopores of the zeolite phase by zinc ferrite particles.

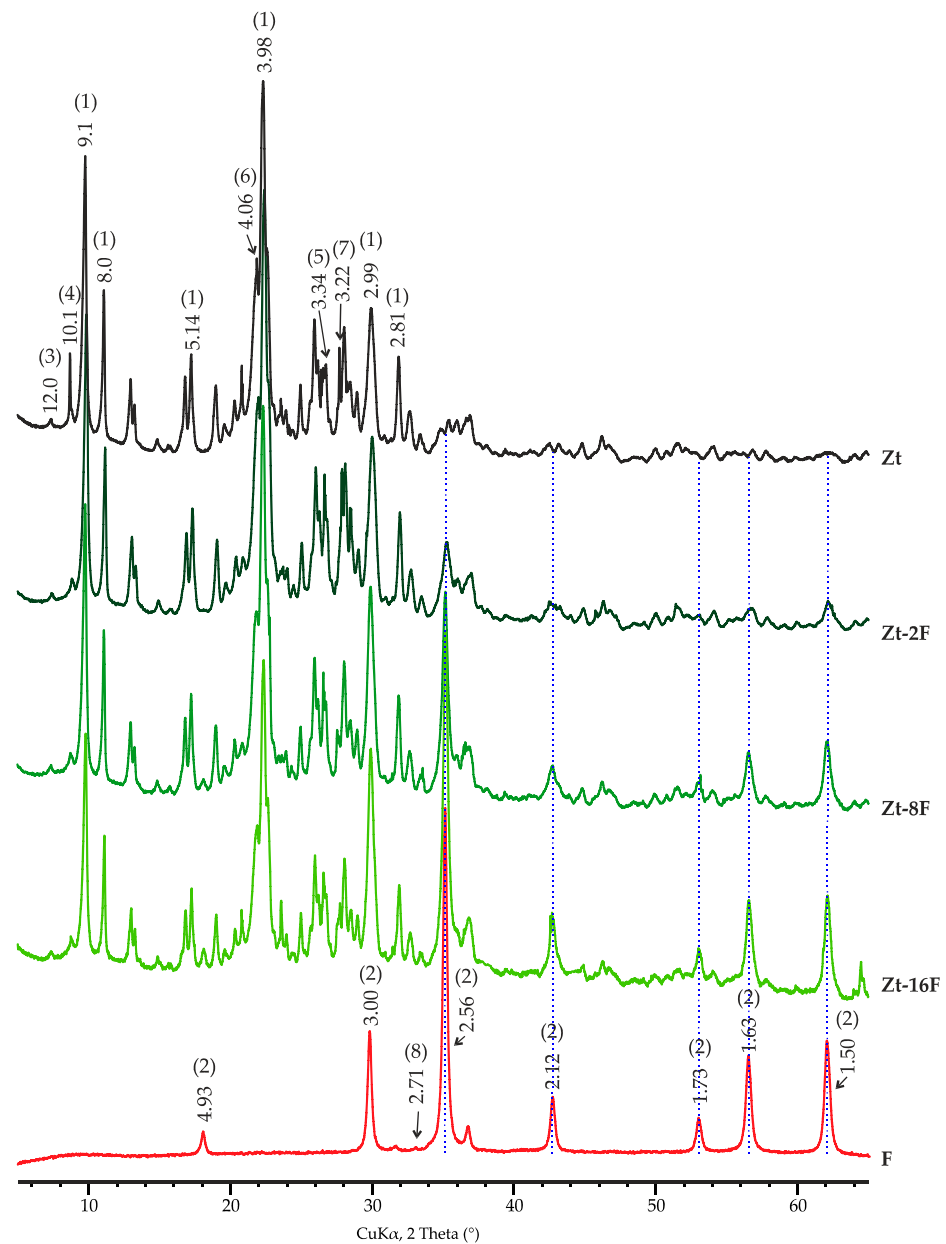


Figure 1. X-ray diffraction patterns of investigated samples of zinc ferrite (F), clinoptilolite (Zt) and composites Zt-2F, Zt-8F and Zt-16F. Phase designation: 1—clinoptilolite, 2— ZnFe_2O_4 , 3—smectite, 4—illite, 5—quartz, 6—crystalite, 7—feldspars, 8—hematite.

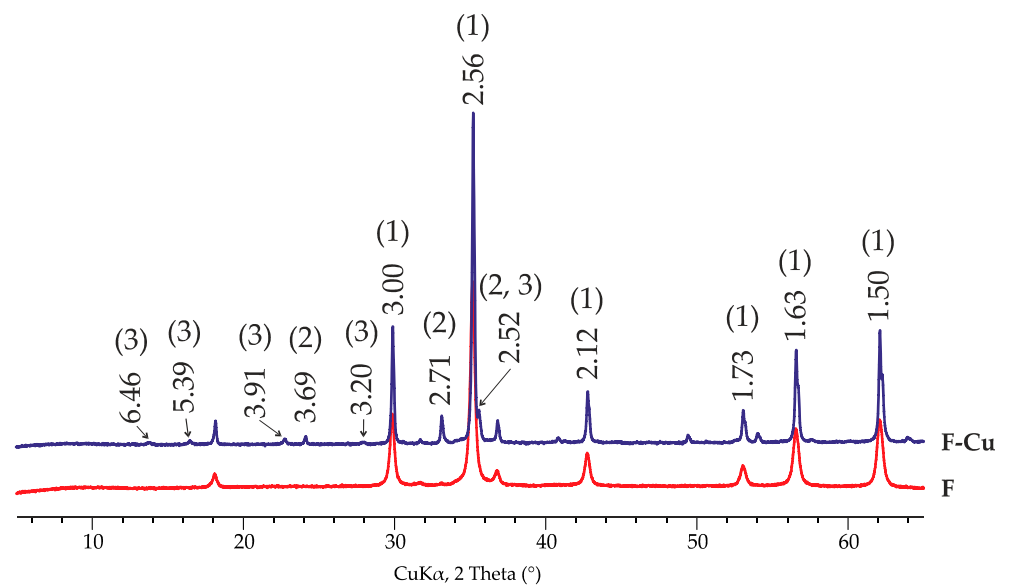


Figure 2. X-ray diffraction patterns of zinc ferrite before (F) and after (F-Cu) sorption of Cu^{2+} : 1— ZnFe_2O_4 , 2—hematite, 3—brochantite.

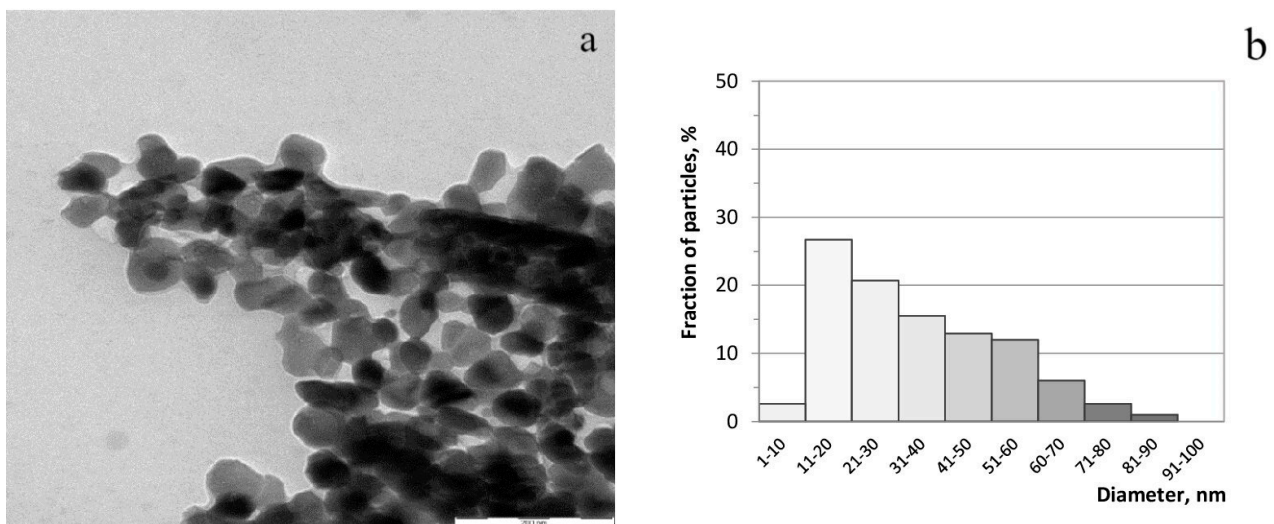


Figure 3. TEM-image of zinc ferrite (a) and histogram of particle size distribution (b).

Table 1. Chemical composition of zeolite, zinc ferrite and composites on their base.

| Sample | Oxide Content, Mass. % | | | | | | | Total |
|--------|------------------------|-------------------------|--------------|----------------------|--------------|-------------------------|--------------|--------|
| | SiO_2 | Al_2O_3 | MgO | K_2O | CaO | Fe_2O_3 | ZnO | |
| Zt | 78.78 | 11.29 | 0.90 | 4.36 | 2.97 | 1.70 | 0.00 | 100.00 |
| Zt-2F | 74.30 | 10.58 | 1.12 | 3.93 | 2.85 | 5.42 | 1.80 | 100.00 |
| Zt-16F | 59.60 | 9.22 | 1.17 | 3.14 | 2.12 | 17.03 | 7.73 | 100.00 |
| F | 1.16 | 0.00 | 0.00 | 0.00 | 0.00 | 62.41 | 36.43 | 100.00 |

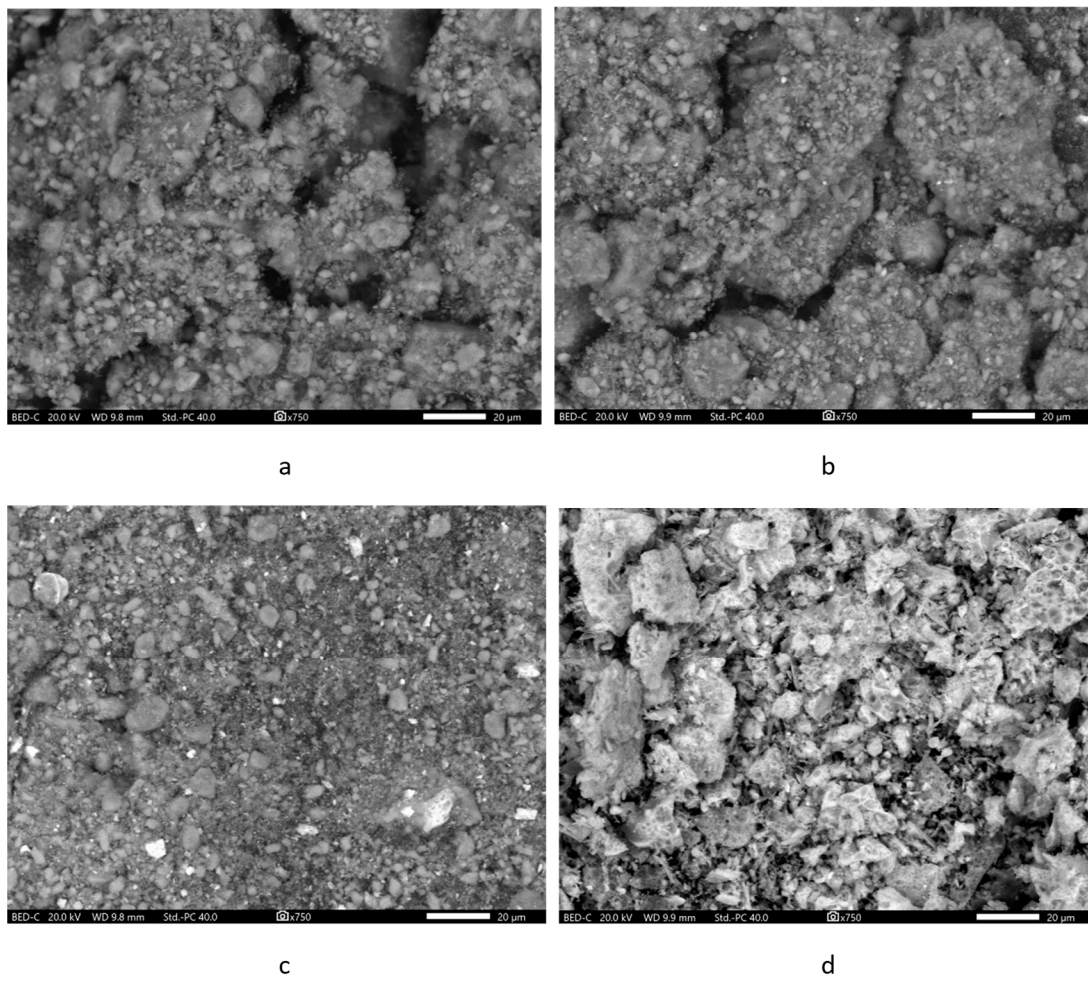


Figure 4. SEM-images of the samples: (a)—Zt, (b)—composite Zt-2F; (c)—composite Zt-16F; (d)—F.

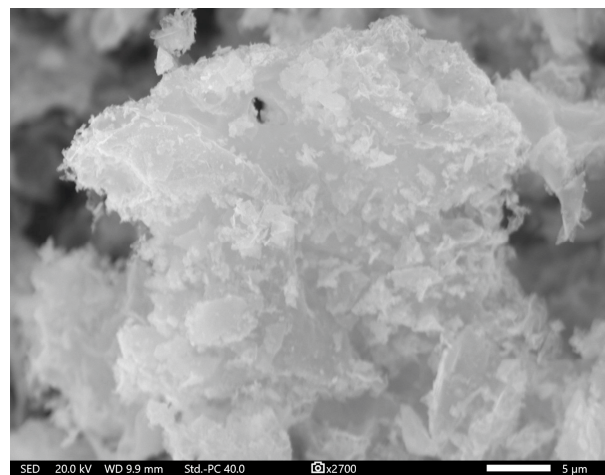


Figure 5. Micrograph of zinc ferrite in secondary electrons.

3.2. Characterization of Surface Morphology of Zeolite, Zinc Ferrite and Composites on their Base

Isotherms of nitrogen adsorption–desorption by investigated samples are given in Figure 6.

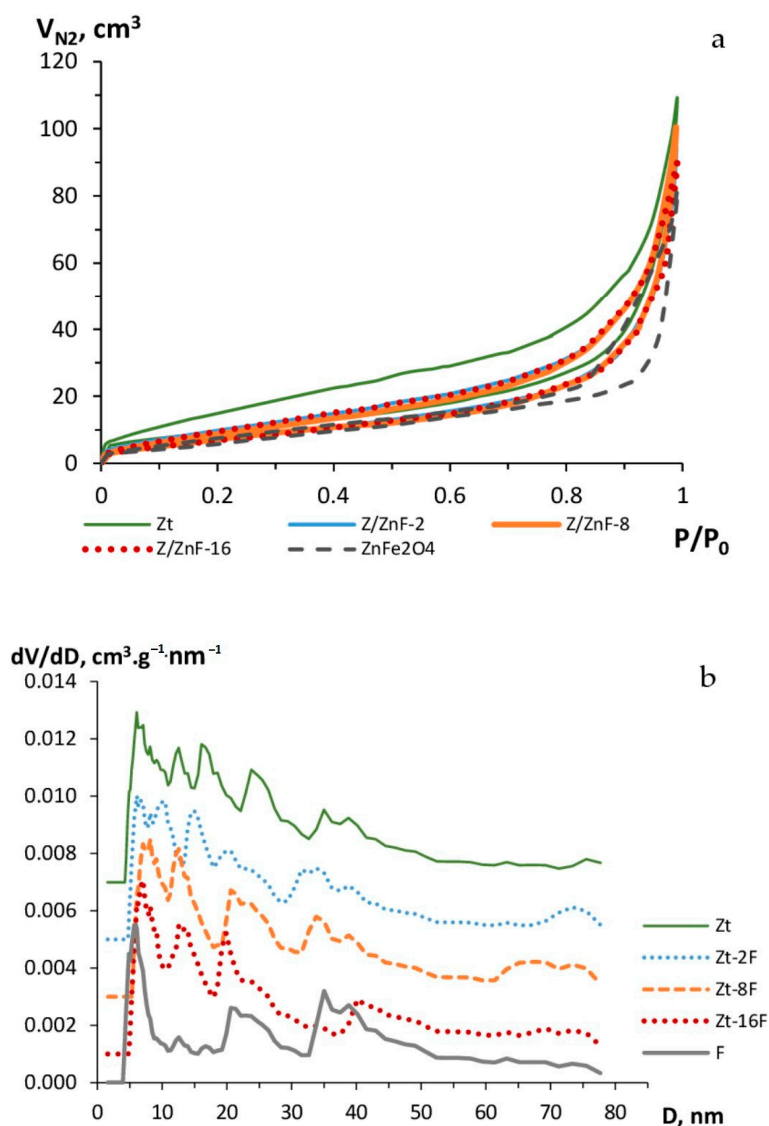


Figure 6. Isotherms of nitrogen adsorption–desorption (a) and pore size distribution (b) of zeolite (Zt), zinc ferrite (F) and composites Zt-2F, Zt-8F and Zt-16F.

The S-shaped view of the nitrogen adsorption–desorption isotherms (Figure 6a) for the investigated samples and the presence of a hysteresis loop correspond to the adsorption isotherms of type IV in the IUPAC classification, thus indicating the occurrence of a polymolecular adsorption in the mesopores of sorbents, which act as the main adsorption pores of the given materials. The minor fraction of micropores present in the investigated samples was marked by a slight rise of the initial section of the isotherms.

The hysteresis loop for the Zt sample was the widest in the whole range of relative pressures, which testified to a broad size distribution of mesopores. For the sample of zinc ferrite (F), the loop of hysteresis was shifted in the range of $P/P_0 = 0.7-1$, which can be due to the presence of larger pores in the given sample. The isotherms of nitrogen adsorption–desorption obtained for samples of composites had a similar view, but differed from the one of the Zt sample by a narrower hysteresis loop, obviously due to a decrease in the size and volume of mesopores by their filling with nanoparticles.

The pore size distribution presented in Figure 6b evidenced the presence of a number of both narrow and larger mesopores in the phase of the studied samples. For the clinoptilolite sample, mesopores were represented by the sizes of about 6, 12 and 16 nm in diameter and larger (25 and 35–45 nm) pores. The mesopores of the zinc ferrite sample were represented

by pores of 5, 20 and 35–40 nm in diameter. As a result of zeolite modification with 2, 8 and 16 mass % of zinc ferrite nanoparticles, the porosity of the composite material markedly changed. By the increase in the content of the ZnFe_2O_4 phase in the composite, the fraction of mesopores with sizes near 16, 25, 35 nm declined in favor of an increasing proportion of mesopores with diameters of 12–14, 19–21 and 30 nm. Moreover, the fraction of macropores for composites Zt-2F and Zt-8F grew, as compared to the Zt sample.

The value of specific surface area, pore volume and pore diameter of the investigated samples are summarized in Table 2.

Table 2. Specific surface area, pore volume and pore diameter of the samples of zeolite, zinc ferrite and composites on their base.

| Sample | S_{BET} , m^2/g | Pore Volume, cm^3/g | | | Pore Diameter, D_{aver} , nm |
|--------|--|-------------------------------------|--------------------|--------------------|---------------------------------------|
| | | V_{meso} | V_{macro} | V_{total} | |
| Zt | 36 | 3.58 | 2.01 | 5.59 | 6.08 |
| Zt-2F | 29 | 3.09 | 1.74 | 4.83 | 6.08 |
| Zt-8F | 31 | 3.05 | 1.84 | 4.89 | 8.15 |
| Zt-16F | 29 | 2.98 | 1.66 | 4.64 | 7.03 |
| F | 26 | 2.18 | 1.46 | 3.64 | 5.88 |

As follows from Table 2, the total pore volume and the value of the specific surface area of zinc ferrite was approximately 1.5 times lower than those of natural zeolite, which accounted for its low porosity. The introduction of the zinc ferrite phase into the composition of composite material on the base of zeolite caused a contraction of total pore volume and specific surface of the material by 12–17%, when compared against the natural clinoptilolite, apparently, due to obstructing the mesopores by modification and the formation of new big pores with a diameter of more than 60 nm (Figure 6b). Figure 4a–c and Figure S1a–c clearly illustrate the filling of pore space and gaps between zeolite aggregates by the particles of the ferrite phase and leveling the relief of the surface.

Thus, the study of physical adsorption of nitrogen revealed a decline in the porosity of the resulting composite material, which, apparently, might affect the intensity and extent of sorption of other sorbates.

3.3. Kinetics of Cu^{2+} Ions' Sorption from Aqueous Solutions by Zeolite, Zinc Ferrite and Composites on Their Base

The regularities of sorption kinetics are determined by the mechanism of sorption uptake and the conditions of the process. The revealing of the kinetic features is necessary to establish the extent of the process and the efficiency of sorption extraction of the sorbate.

The kinetic curves of Cu^{2+} ions' sorption by the samples of zeolite, zinc ferrite and composites based on them are shown in Figure 7.

As follows from Figure 7, the sorption process at the specified sorbents developed relatively quickly, leading to reaching the equilibrium in 5–10 min for the samples of Zt and Zt-2F, and over 30–40 min for samples of composites Zt-8F, Zt-16F and zinc ferrite (F), which is in agreement with the available data [70,71].

For zeolites, the process of ion-exchange uptake of cations from an external solution typically proceeds rather quickly. For ferrites, the sorption process can be carried out due to the contribution of both electrostatic interactions and redox or other chemical reactions [34,71–73].

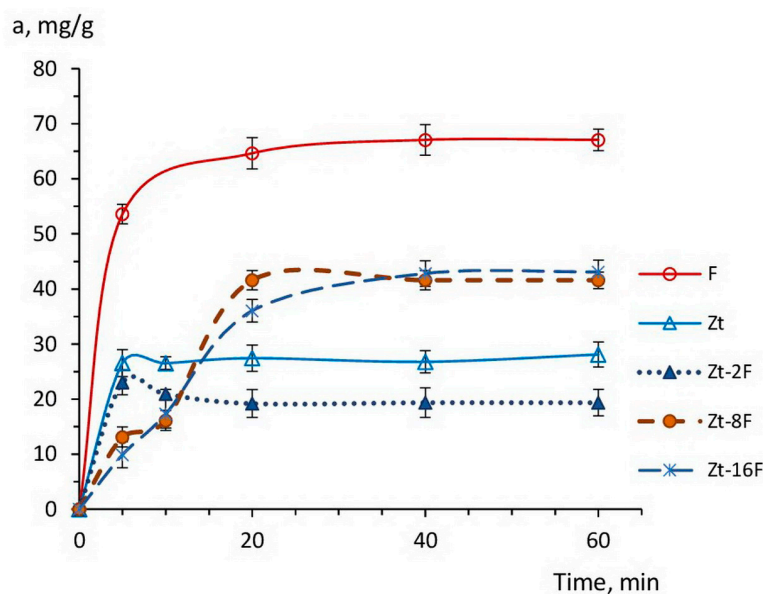


Figure 7. Kinetic curves of Cu^{2+} ions sorption by the samples of zeolite (Zt), zinc ferrite (F) and composites Zt-2F, Zt-8F, Zt-16F from 0.01 N CuSO_4 solution.

It is noteworthy that throughout the entire range of the kinetic curve, the sorption capacity of zinc ferrite sample was 2–2.5 times higher than the capacity of natural zeolite, which indicated a high affinity of the zinc ferrite surface for copper ions. Apparently, the free access of active sites, i.e., oxygen anions, at the developed surface of ferrite nanoparticles contributed to the high adsorption of sorbate ions, although, in solutions with low pH, a competitive adsorption of protons was noticeable [6,34,74].

The sorption capacity of zeolites is restricted by their ion exchange capacity, which, for natural clinoptilolites, is in the order of 0.4–2.2 meqv/g [75,76]. For the studied sample of clinoptilolite, the value of the exchange capacity was ~ 0.8 meqv/g [77], which provided an equivalent extraction of copper cations in the amount of 25.6 mg/g and coincides with the experimental adsorption value shown in Figure 7 for zeolite.

The introduction of 2% of the ZnFe_2O_4 phase into the composite caused a somewhat lowering of its sorption capacity as compared to zeolite (Zt), apparently due to the blocking of transport pores and the access to exchange cations within the zeolite phase. However, a further increase in the content of the ferrite phase in the composition of composite to 8 and 16%, on the contrary, led to the incrementing sorption capacity of the composite sorbent, despite the abatement of the porosity and specific surface area found in Section 3.2 (Figure 6).

This fact indicated a decisive contribution of the zinc ferrite phase to the process of Cu^{2+} sorption. Similar behavior was discovered for composite sorbents based on bentonite and cobalt ferrite [72], for which a 15% addition of cobalt ferrite in the composite (0.85B/0.15CF) was optimal and provided the highest value of heavy metal ion adsorption.

For the characterization of the mechanism of sorption extraction of copper ions from aqueous solution by the investigated sorbents, experimental kinetic curves were described, applying models of pseudo-first and pseudo-second order in the form of next kinetic equations [68,69]:

$$\log(q_e - q_t) = \log q_e - \frac{k_1 \cdot t}{2.303} \quad (6)$$

$$\left(\frac{t}{q \cdot t}\right) = \frac{1}{k_2 \cdot (q_e)^2} + \left(\frac{t}{q_e}\right) \quad (7)$$

where q_t and q_e —amounts of Cu^{2+} ions (in mg/g of sorbent) sorbed by the moment of time t and the moment of equilibrium, correspondingly; K_1 —rate constant of sorption of

pseudo-first order ($\text{g}\cdot\text{mg}^{-1}\cdot\text{min}^{-1}$); K_2 —rate constant of sorption of pseudo-second order ($\text{g}\cdot\text{mg}^{-1}\cdot\text{min}^{-1}$); V —volume of solution, dm^3 ; m —mass of sorbent (g); and t —contact time (min).

The linear approximation of the experimental data confirmed that the pseudo-second order model described the kinetics of the process under study in the best way ($R^2 = 0.99$ –1) (Table 3). Therefore, the rate of adsorption of copper ions on the surface of the studied sorbents depended on the number of adsorption sites [1] and was controlled by the contribution of the chemical reaction [2,74].

Table 3. Kinetic parameters of sorption of Cu^{2+} ions by the samples of zeolite, zinc ferrite and composites on their base.

| Sample | Equation | Parameters of Pseudo-Second Order Model | | | |
|--------|------------------------|---|---|--------|--------|
| | | q_{e2} , mg/g | k_2 , $\text{g}\cdot\text{mg}^{-1}\cdot\text{min}^{-1}$ | R^2 | RMSE |
| Zt | $y = 0.0354x + 0.0261$ | 28.25 | 0.0480 | 0.9994 | 0.0192 |
| F | $y = 0.0145x + 0.0271$ | 68.97 | 0.0078 | 0.9993 | 0.0119 |
| Zt-2F | $y = 0.0514x + 0.012$ | 19.45 | 0.0560 | 1.0000 | 0.0024 |
| Zt-8F | $y = 0.0201x + 0.19$ | 49.75 | 0.0021 | 0.9672 | 0.0767 |
| Zt-16F | $y = 0.0209x + 0.1237$ | 47.85 | 0.0035 | 0.9972 | 0.0182 |

The values of the pseudo-second order rate constant calculated from the kinetic equation for the samples Zt and Zt-2F were 6–7 times higher than for the sample F, and more than 13–16 times higher than those for the composites Zt-8F and Zt-16F. This fact testified to the lower rates of the sorption process, in the cases of the pure zinc ferrite sample and the composites Zt-8F and Zt-16F, for which the chemical reaction controls the overall sorption process.

The elemental mapping of the samples (Figures 8 and S2) after the adsorption of Cu^{2+} ions indicated a uniform distribution of copper on the surface of the samples.

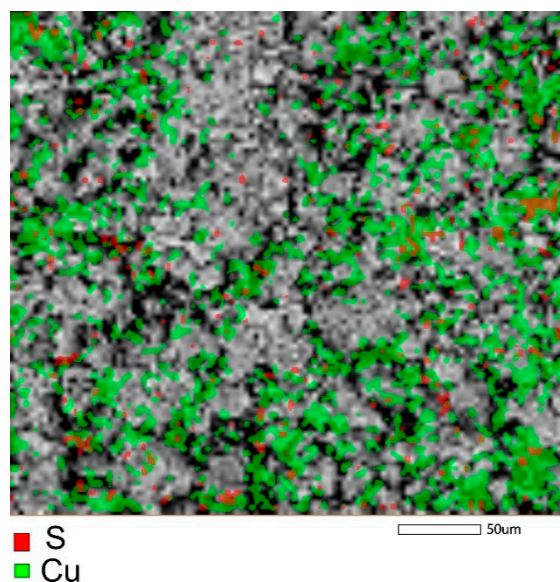


Figure 8. Mapping of copper and sulfur in the sample of zinc ferrite after adsorption of Cu^{2+} from aqueous solution.

From the comparison of the elemental composition of the samples (Table 4) determined from EDS-analysis, it may follow that, namely, the phase of zinc ferrite had a significant contribution to the uptake of copper by the sample of composite Zt-16F. An enhanced affinity for copper ions was also found in [73] for the sample of calcium ferrite.

Table 4. Elemental composition of zeolite, zinc ferrite and composite Zt-16F after sorption of Cu^{2+} -ions.

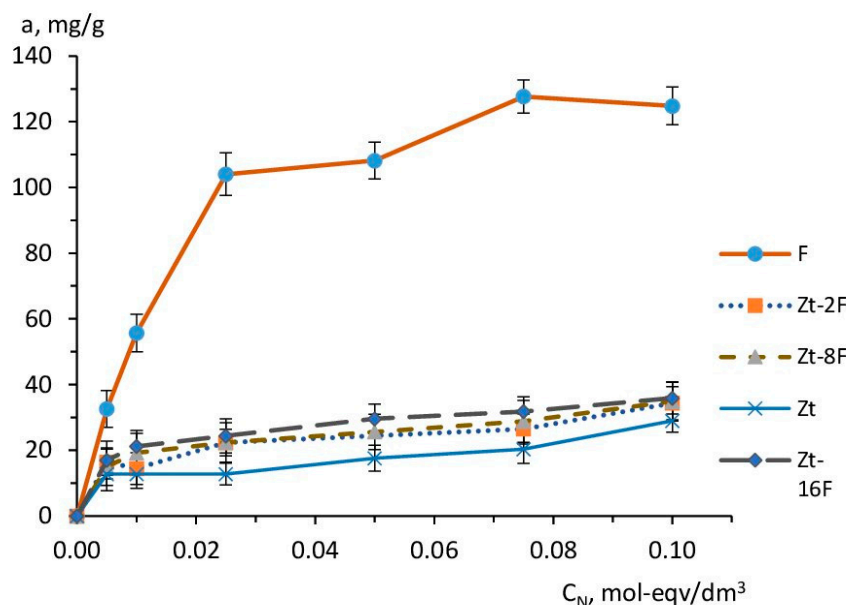
| Sample | Mass.% | | | | | | | | | Total |
|--------|--------|------|-------|------|------|-------|------|-------|-------|--------|
| | Mg | Al | Si | K | Ca | Fe | Cu | Zn | O | |
| Zt-Cu | 0.51 | 6.19 | 36.15 | 3.16 | 2.06 | 2.07 | 0.38 | - | 49.48 | 100.00 |
| Zt-16F | 0.48 | 4.72 | 25.67 | 2.49 | 1.34 | 13.51 | 0.74 | 8.25 | 42.81 | 100.00 |
| F | - | 0.43 | 1.52 | - | - | 41.74 | 1.15 | 27.97 | 27.19 | 100.00 |

As shown in [78,79], the surface of catalysts based on ZnFe_2O_4 possessed a dual nature and exhibited the properties of both Lewis acids, due to the strong electron-withdrawing properties of the Fe^{3+} cation in octahedral positions, and Lewis bases, due to the oxygen anions O^{2-} located at the nodes of the spinel crystal lattice. In addition, Zn^{2+} ions occupying tetrahedral positions in the lattice act as an activator of π -bonds that, along with the acid–base nature of zinc ferrites, exhibited a serious catalytic effect in multicomponent reactions [80]. Taking this into consideration, one may assume that hydrated copper cations are predominantly adsorbed on the surface of zinc ferrite due to electrostatic interaction with oxygen anions, O^{2-} . A similar situation was also found in [74] by the investigation of Zn^{2+} adsorption on the surface of MnFe_2O_4 and CoFe_2O_4 adsorbents.

The extent of sorption can be estimated from the adsorption isotherms discussed below.

3.4. Isotherms of Cu^{2+} Ions' Sorption by Samples of Zeolite, Zinc Ferrite and Composites on Their Base

The adsorption equilibrium in the system “sorbent-sorbate” and the sorption capacity of the sorbent were experimentally studied using the experimental isotherms of copper ion sorption shown in Figure 9 and obtained at 40 min time of sorption equilibrium establishment.

**Figure 9.** Isotherms of Cu^{2+} sorption by sorbents based on zeolite (Zt), zinc ferrite (F) and composites Zt-2F, Zt-8F, Zt-16F.

According to Figure 9, the experimental sorption isotherms have a convex character at the initial stage of the process, indicating the predominance of “sorbent-sorbate” interactions. The isotherm for the zinc ferrite sample (F) was much higher than the isotherms for other samples, thus illustrating a higher affinity of this sorbent sample for Cu^{2+} ions. This

isotherm reached saturation at high concentrations and was similar in configuration to isotherms of type I, according to the IUPAC classification. A similar type of isotherm was also found in [74] for samples of MnFe_2O_4 and CoFe_2O_4 adsorbents, and in [31] for $\text{ZnFe}_2\text{O}_4@BC$ and $\text{MnFe}_2\text{O}_4@BC$ composites based on zinc ferrite, manganese ferrite and biochar.

Sorption isotherms for samples Zt, Zt-2F and Zt-8F were significantly lower than for the sample F and differed in configuration from isotherms of type I, since the sorption value (a , mg/g) did not reach its limiting value, but continued rising, with an increase in the concentration of the equilibrium solution. This can be caused by the occurrence of the polymolecular adsorption due to “sorbate-sorbate”-type interactions. The limited value of the exchange capacity of zeolite caused the lowest course of the sorption curve of Cu^{2+} ions for zeolite sorbent (Zt). However, in the region of higher concentrations, similarly to the samples of composite sorbents, the superequivalent absorption of sorbate ions was manifested for Zt.

In the range of medium and high concentrations of the equilibrium solution, the sorption capacity of the studied sorbents differed markedly and decreased in the order: $F > \text{Zt-16F} > \text{Zt-8F} \approx \text{Zt-2F} > \text{Zt}$. It is important to note that the obtained trend had an inverse correlation with the value of the specific surface area S_{BET} , m^2/g : $\text{Zt} > \text{Zt-16F} \approx \text{Zt-8F} \approx \text{Zt-2F} > F$ and the porosity of the samples, determined by the value of low-temperature (physical) nitrogen adsorption (Table 2). Therefore, the sorption process with the participation of zinc ferrite samples and composites containing the ferrite phase differed from the physical adsorption and was implemented according to a different mechanism, the contribution of which became stronger at higher content of the ferrite phase [31,74]. In the case of the natural zeolite clinoptilolite, the mechanism of sorption of copper ions was predominantly an ion-exchange.

The regularities of adsorption on homogeneous surfaces and in the case of porous adsorbents are different, since the state of the surfaces is energetically not the same. Adsorption on a homogeneous solid surface is described by Langmuir’s theory of monomolecular adsorption. Adsorption on a heterogeneous surface with varied affinities of active sites for the sorbate and a nonlinear isotherm is described by the Freundlich model.

In order to characterize the equilibrium of sorption, experimental isotherms were approximated by the linear equations of the Langmuir (7) and Freundlich (8) adsorption models in the following view:

$$\frac{1}{a} = \frac{1}{a_{\text{max}} \cdot K_L} \cdot \frac{1}{C_{\text{eq}}} + \frac{1}{a_{\text{max}}} \quad (8)$$

$$\log a = 1/n \log C + \log K_F, \quad (9)$$

where a —adsorption capacity of sorbent at equilibrium, a_{max} —maximal adsorption (mg/g), C_{eq} —equilibrium adsorbate concentration in solution (mg/dm^3); K_L —equilibrium constant of Langmuir (dm^3/mg), K_F —Freundlich equilibrium constant (dm^3/mg), C and $1/n$ —constants of the Freundlich equation.

Experimental isotherms were plotted in the linear coordinates of Langmuir ($1/a$ vs. $1/C_{\text{eq}}$) and Freundlich ($\log a$ vs. $\log C_{\text{eq}}$) equations, linearized and subsequent parameters of the linear equations (slope k and intercept b) were used to determine the corresponding parameters of the Langmuir (a_{max} and K_L) and Freundlich (n and K_F) equations, presented in Table 5.

Table 5. Equation parameters of the adsorption models of Langmuir and Freundlich determined for copper ions' sorption by investigated sorbents.

| Sample | Langmuir Model | | | | Freundlich Model | | | |
|--------|----------------------|----------------|-------------------------|----------------|----------------------|----------------|------|----------------|
| | Linear Equation | R ² | a _{max} , mg/g | K _L | Linear Equation | R ² | n | K _F |
| Zt | y = 0.0055x + 0.0515 | 0.4741 | 19.42 | 9.36 | y = 0.2429x + 1.2351 | 0.735 | 4.17 | 17.18 |
| F | y = 0.0039x + 0.0062 | 0.9928 | 161.3 | 1.59 | y = 0.4435x + 1.9409 | 0.9118 | 2.25 | 87.28 |
| Zt-2F | y = 0.0052x + 0.0366 | 0.6191 | 27.32 | 7.04 | y = 0.2564x + 1.3621 | 0.8703 | 3.9 | 23.02 |
| Zt-8F | y = 0.0056x + 0.0331 | 0.9234 | 30.21 | 5.91 | y = 0.249x + 1.3825 | 0.9666 | 4.02 | 24.13 |
| Zt-16F | y = 0.0048x + 0.0305 | 0.9329 | 32.79 | 6.35 | y = 0.2337x + 1.4239 | 0.9885 | 4.28 | 26.54 |

As follows from Table 5, the high values of the correlation coefficients and the nature of the obtained isotherms with saturation (for F sample) evidenced that the Langmuir model successfully described the sorption process on the sample of zinc ferrite (F), like that found for composites based on metal ferrites [31,74].

The higher correlation coefficients of the Freundlich model were found for the sorption isotherms on zeolite (Zt) and all samples of composites Zt-2F, Zt-8F and Zt-16F, which may indicate the heterogeneous nature of the surface of these sorbents, as well as the possibility of polymolecular sorption.

For all of the samples, the values of constant n of the Freundlich equation were $n > 1$, indicating the favorable sorption conditions. The value of K_F was the highest for the ferrite sample (F), specifying its greater affinity for the sorbate compared to zeolite (Zt).

However, the values of the sorption equilibrium constant K_L, determined from the Langmuir model, testified the higher energy of sorption interaction in case of zeolite and composite samples, rather than in the case of sample F.

The sorption capacity of the resulting ZnFe₂O₄/zeolite composites can be compared with other composite metal ferrite-based sorbents using the data of Table 6.

Table 6. Adsorption capacity of metal ferrite-based composites for heavy metals ions.

| Metal Ferrite-Based Composite | Type of Heavy Metal | Adsorption Capacity, (mg/g) | Reference |
|--|---------------------|-----------------------------|-----------|
| Cobalt-ferrite nanocomposite (CFNC) | Cr(III) | 217.00 | [14] |
| | Cd(II) | 303.00 | |
| Manganese ferrite nanoparticles (NPs) | As(III) | 49.05 | [16] |
| | As(V) | 27.65 | |
| Cobalt-zinc ferrites NPs (Co _x Zn _{1-x} Fe ₂ O ₄) | Pb | 289.00 | [21] |
| | Pb | 275 | |
| CoFe ₂ O ₄ NPs | Zn | 390 | [20] |
| | Zn | 454.5 | |
| MnFe ₂ O ₄ | Cr | 30.00 | [79] |
| Iron-nickel oxide | Cd | 160.91 | [81] |
| | Ni | 49.42 | |
| Mixed oxides and ferrites nanoparticles | Cd | 54.69 | [33] |
| | Cr | 12.34 | |
| Amine-functionalized MgFe ₂ O ₄ | Pb | 32.2 | [34] |
| | Pb | 66.0 | |
| Bentonite/CoFe ₂ O ₄ /hydroxyapatite | Cu | 44.73 | [82] |
| | Pb | 247.14 | |
| MK100, clinoptilolite metakaolin based geopolymer | Cd | 74.36 | [83] |
| | Zn | 30.52 | |
| | Cr | 21.84 | |
| Fe ₃ O ₄ -hydroxyapatite | Cu | 48.78 | [83] |
| | Ni | 29.07 | |
| CuFe ₂ O ₄ @HAp | Fe (II) | 91.7 | [84] |
| | Al (III) | 49.2 | |
| PVA-barium ferrite composite | Pb | 3.96 | [85] |
| | Cd | 2.51 | |
| | Cu | 4.06 | |

Table 6. Cont.

| Metal Ferrite-Based Composite | Type of Heavy Metal | Adsorption Capacity, (mg/g) | Reference |
|---|----------------------------|--------------------------------|-----------|
| PVA–nickel ferrite composite | Pb | 4.67 | [85] |
| | Cd | 1.07 | |
| | Cu | 4.14 | |
| MnFe ₂ O ₄ /Chitosan | Cu (II) | 14.86 | [86] |
| | Pb (II) | 15.36 | |
| Reduced graphene oxide–cobalt ferrite nanocomposite, RGCF | As (V) | 222.2 | [87] |
| Rice Straw-CoFe ₂ O ₄ | Fe, Mn, Cu, Cd, Zn, Ni, Pb | Removal efficiency, R = 20–55% | [88] |
| Nickel ferrite carboxymethyl cellulose composite (NiFCMC) | Ni | 47.84 | [89] |
| Nickel ferrite–carboxymethyl cellulose–sodium alginate bio-composite (NiFCMC-Alg) | Ni | 60.24 | [89] |
| BiFeO ₃ /Ni _{0.1} Fe _{2.9} O ₄ nanocomposites | Cr (VI) | Removal efficiency, R = 75% | [90] |

The next section considers the effectivity of the studied samples of nanosorbents in the water purification from heavy metal ions.

3.5. Effectiveness of Water Purification and Regeneration of Sorbents

The calculated values of the degree of water purification (R, %), indicating the extent of Cu²⁺ ion extraction from the model solution with 320 mg/dm³ of copper ion content, are shown in Figure 10.

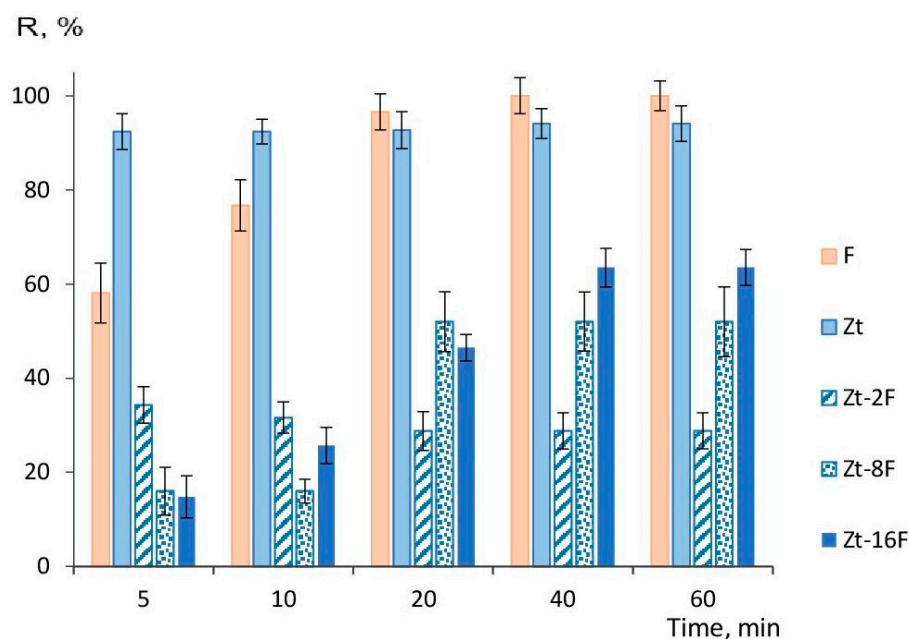


Figure 10. Degree of water purification from Cu²⁺-ions by samples of sorbents at varied sorption times: F—zinc ferrite; Zt—zeolite; Zt-2F, Zt-8F and Zt-16F—composites based on zeolite with 2, 8 and 16% content of zinc ferrite.

It follows from Figure 10 that sorbents based on natural zeolite provided a high degree of water purification (92–94%), regardless of the duration of the sorption process. The sorbent based on zinc ferrite reached the highest efficiency at a sorption time of 40 min and was able to provide 100% extraction of copper ions from the solution. Under given conditions, the efficiency of purification of the model solution from copper ions by the composite sorbents was significantly lower (2–3 times), apparently due to a decreased

number of available pores for transport of sorbate to surface sites of the sorbent. Therefore, to raise the efficiency of water purification, it is necessary to increase the amount of sorbent. It was shown in [14] that the amount of 10–15 g/L of a magnetic composite sorbent based on cobalt ferrite was insufficient to provide a high degree of purification, while 20 g/L arrived at 100% purification.

To recommend the sorbents for practical use, the possibility of their regeneration using a number of electrolyte solutions, e.g., 0.1 N NaCl, NaOH and HCl, was studied. It was found that in case of the samples of zinc ferrite (F) and composites Zt-8F and Zt-16F, solutions of 0.1 N sodium chloride and sodium hydroxide did not lead to desorption of the sorbate and cannot be used to regenerate sorbents, in contrast to [71], where the sorbent based on ferrite nanoparticles of various metals, except for manganese ferrite, was successfully regenerated with 0.01 N NaOH.

In the case of using 0.1 N HCl solution as an eluent for the sample of zinc ferrite (F), a complete desorption of adsorbed copper in an equivalent amount was found (Table S2). This was consistent with [74], in which 0.1 M HCl solution was determined to be the most effective for the regeneration of a sorbent based on MnFe_2O_4 and CoFe_2O_4 , while solutions of H_2SO_4 and HNO_3 manifested the least destructive effect on the sorbent. As for the possibility of regeneration of another effective sorbent, clinoptilolite (Zt) and zeolites, as representatives of inorganic ion-exchangers, can be regenerated easily with solutions of high concentrations of acids (>1 M) or other electrolytes. In our case, regeneration of the Zt sample with 0.1 N HCl resulted in desorption of 60% of the adsorbed amount of copper ions.

In the absence of regeneration, as was experimentally determined for the samples of zinc ferrite (F) and composites Zt-8F and Zt-16F, the sorption capacity gradually decreased with each new operating cycle (Figure 11), but, nevertheless, allowed using the sorbents in two to three sorption cycles.

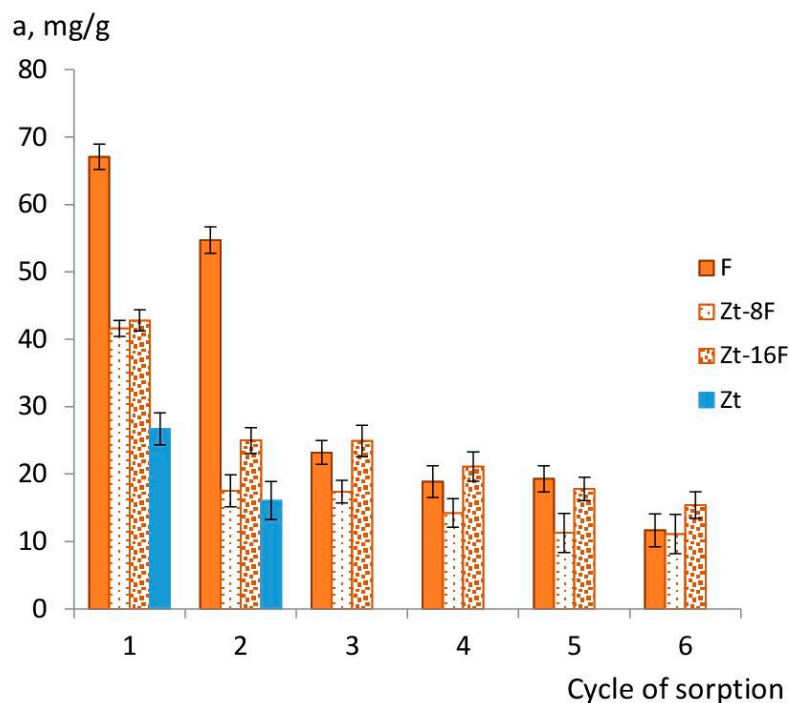


Figure 11. Sorption capacity of sorbents depending on number of sorption cycles from 0.01 N CuSO_4 solution. *Note.* F, Zt-8F, Zt-16F—without regeneration; Zt—2nd cycle of sorption after regeneration by 0.1 N HCl; Zt-8F—6th cycle after regeneration by 0.1 N HCl.

Figure 11 illustrated that sorbents based on zinc ferrite were able to successfully purify the aqueous phase during two to three operating cycles without regeneration. Subsequently,

it is recommended to restore the sorption capacity of sorbents by their regeneration with 0.1 N HCl solution. According to [14], another possible way to regenerate the sorbent based on metal ferrites can be a mixture of ethanol/methanol (1:1), which made it possible to use the sorbent for 4 cycles.

Among the samples of composite materials, the Zt-16F composite was the most effective in terms of the degree of water purification upon reaching the sorption equilibrium; its capacity was only 30–35% lower than one for F and Zt sorbents. However, an indisputable advantage of the new composite nanosorbents was their acquisition of magnetic properties and a unique ability to be extracted after the completion of the adsorption cycle, which will be discussed in the next section.

3.6. Magnetic Properties of the Sorbents

Considering the fact that materials based on zinc ferrite exhibit the properties of magnetically soft materials, the behavior of nanosorbents based on zinc ferrite under the action of an external magnetic field was experimentally studied (Figure 12).

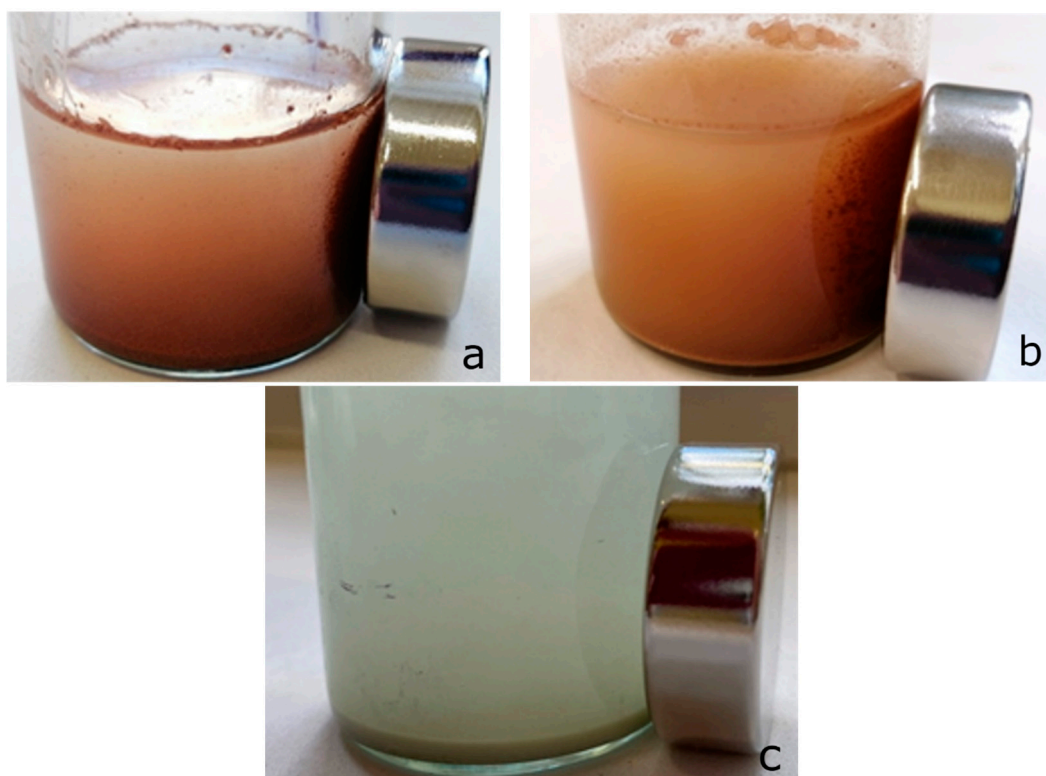


Figure 12. Effect of Nd magnet on suspensions sorbent-0.01 N CuSO_4 solution: (a) zinc ferrite; (b) composite Zt-16F; (c) zeolite.

Figure 12 clearly testifies the ability of zinc ferrite samples, as well as the Zt-16F composite sorbent, for magnetic separation from the equilibrium solution under the action of external magnetic field from the Nd magnet. Compared to natural zeolite and other materials possessing no such activity, the acquisition of magnetic properties by the ZnFe_2O_4 /zeolite composite, owing to the zinc ferrite component, is an undoubted advantage [7,91].

As follows from Figure 13, there was a linear dependence of the magnetic moment on the magnetic field detected, for all of the samples studied, that is distinctive for small concentrations of superparamagnetic particles. The magnetization of ZnFe_2O_4 in the field of 16,000 Oe was about 2.5 emu/g. For the samples of composites, magnetization values were significantly lower than for the F sample, nevertheless, tending to increase with the

rising of the content of the zinc ferrite phase in the composite, and, as a result, imparting the samples of composites Zt-8F and Zt-16F the ability for magnetic separation by an external magnetic field. The magnetic activity of the samples significantly facilitates separation of the spent sorbent for subsequent regeneration and reuse, and preventing its loss, which, by these means, ensures the intensification and improvement of the sorption technology of water purification.

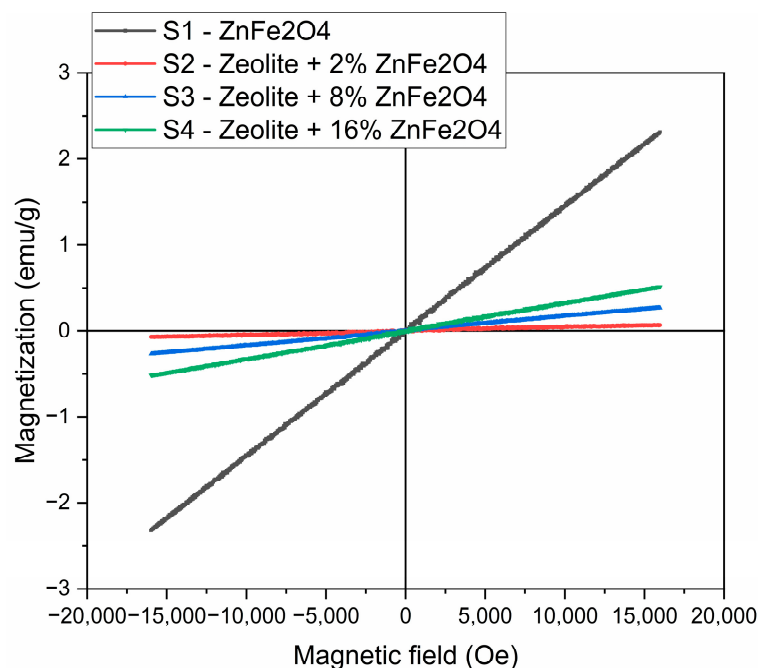


Figure 13. Magnetization curves of zinc ferrite and composites Zt-2F, Zt-8F and Zt-16F samples.

4. Conclusions

New nanocomposite materials with magnetic properties and enhanced sorption capacity for copper ions were obtained on the base of natural zeolite and zinc ferrite nanoparticles, applying the facile synthesis method. Using X-ray diffraction, SEM and BET nitrogen adsorption/desorption methods, it was confirmed that the formation of composites occurred due to changes in the morphology and porosity of the material. Nanoparticles of zinc ferrite embedded the pore space of zeolite and caused a decrease in the specific surface area of composites and their ability for physical adsorption. However, the introduction of 8 and 16 mass % of zinc ferrite phase into the composite improved the sorption ability of the material for copper ions in aqueous medium, due to the implementation of both ion-exchange (zeolite component) and chemisorption (zinc ferrite phase) mechanisms. The sorption capacity of the composites for copper ions was more than 1.5 times higher than the capacity of natural zeolite and increased from 19.42 for zeolite to 32.79 mg/g for the Zt-16F composite.

The kinetic regularities of copper ions' sorption by the studied materials were successfully described by the pseudo-second order model. The equilibrium of the sorption process on the surface of zinc ferrite was adequately described by the Langmuir model, while, for samples of zeolite and composites, the Freundlich model was more suitable.

The efficiency of water purification from copper ions by the developed composite sorbents was quite high, but was inferior to zeolite and zinc ferrite. The limitation of these studies is the applied sorbent/solution ratio, which was not further optimized. By increasing the amount of sorbent, the removal efficiency can be increased to a higher degree. However, the stated ability of these sorbents to operate in several cycles without regeneration, the possibility of successful regeneration and the magnetic properties are those

important advantages that allow recommending ZnFe₂O₄/zeolite composite materials as prospective sorbents of heavy metals.

In the future studies of such materials, attention will be paid to enhancing the magnetic properties of composites by changing their composition, as well as to the multi-component composition of real wastewaters, and assessment of the sorption efficiency of materials in relation to other heavy metals.

Supplementary Materials: The following supporting information can be downloaded at: <https://www.mdpi.com/article/10.3390/appliedchem3040029/s1>, Figure S1: SEM-images of zeolite (a), composite Zt-2F (b), composite Zt-16F (c) and zinc ferrite (d); Figure S2: EDX elemental mapping of copper after adsorption of Cu²⁺ from solution at the surface of investigated samples: a—Zt-Cu; b—Zt-16F-Cu; c—F-Cu; Table S1: pH of aqueous solutions of CuSO₄ at t = 20 °C; Table S2. Desorption of Cu²⁺ from ZnFe₂O₄ sample by various electrolyte solutions.

Author Contributions: Conceptualization, L.N. and E.T. (Elena Tomina); methodology, L.N., E.T. (Elena Tomina), V.K., E.T. (Ekaterina Tyupina) and N.P.; investigation, L.N., A.K., A.M., I.M., T.K., E.T. (Ekaterina Tyupina) and Y.A.; resources, L.N., E.T. (Elena Tomina), V.K. and E.T. (Ekaterina Tyupina); writing—L.N. and E.T. (Elena Tomina); writing—Review and Editing, L.N., E.T. (Elena Tomina), V.K., I.M., T.K., E.T. (Ekaterina Tyupina) and N.P.; visualization, L.N., E.T. (Elena Tomina) and V.K.; supervision, E.T. (Elena Tomina) and L.N.; project Administration, E.T. (Elena Tomina); funding Acquisition, E.T. (Elena Tomina) and V.K. All authors have read and agreed to the published version of the manuscript.

Funding: This research was funded by the Russian Science Foundation, grant No. 23-23-00122, and grant No. 22-17-00252 for the methodological developments of the detailed identification of the mineral composition.

Data Availability Statement: The data presented in this study are available in the article and in the Supplementary Material.

Acknowledgments: The authors would like to thank you Nataliya Truskova for the valuable support in the laboratory during the implementation of the experiments on adsorption and Nikolay Kurkin for technical assistance.

Conflicts of Interest: The authors declare no conflict of interest.

References

1. Teng, D.; Jin, P.; Guo, W.; Liu, J.; Wang, W.; Li, P.; Cao, Y.; Zhang, L.; Zhang, Y. Recyclable Magnetic Iron Immobilized onto Chitosan with Bridging Cu Ion for the Enhanced Adsorption of Methyl Orange. *Molecules* **2023**, *28*, 2307. [CrossRef]
2. Fito, J.; Tibebe, S.; Nkambule, T.T.I. Optimization of Cr (VI) removal from aqueous solution with activated carbon derived from *Eichhorniacrassipes* under response surface methodology. *BMC Chem.* **2023**, *17*, 4. [CrossRef] [PubMed]
3. Sviridova, E.S.; Kolesova, Y.A.; Voronyuk, I.V.; Eliseeva, T.V.; Mukhin, V.M. Features of sorption of hydroxybenzaldehydes from aqueous solutions with activated carbon VSK-400. *Sorbtsionnye I Khromatograficheskie Protssesy* **2022**, *22*, 901–908. [CrossRef]
4. Jaspal, D.; Malviya, A. Composites for wastewater purification: A review. *Chemosphere* **2020**, *246*, 125788. [CrossRef] [PubMed]
5. Dotto, G.L.; McKay, G. Current scenario and challenges in adsorption for water treatment. *J. Environ. Chem. Eng.* **2020**, *8*, 103988. [CrossRef]
6. Soliman, N.K.; Moustafa, A.F. Industrial solid waste for heavy metals adsorption features and challenges: A review. *J. Mater. Res. Technol.* **2020**, *9*, 10235–10253. [CrossRef]
7. Buzukashvili, S.; Hu, W.; Sommerville, R.; Brooks, O.; Kökkılıç, O.; Rowson, N.A.; Ouzilleau, P.; Waters, K.E. Magnetic Zeolite: Synthesis and Copper Adsorption Followed by Magnetic Separation from Treated Water. *Crystals* **2023**, *13*, 1369. [CrossRef]
8. Santamaría, L.; López-Aizpún, M.; García-Padial, M.; Vicente, M.A.; Korili, S.A.; Gil, A. Zn-Ti-Al layered double hydroxides synthesized from aluminum saline slag wastes as efficient drug adsorbents. *Appl. Clay Sci.* **2020**, *187*, 105486. [CrossRef]
9. Saveleva, M.S.; Eftekhari, K.; Abalymov, A.; Douglas, T.E.L.; Volodkin, D.; Parakhonskiy, B.V.; Skirtach, A.G. Hierarchy of Hybrid Materials—The Place of Inorganics-in-Organics in it, Their Composition and Applications. *Front. Chem.* **2019**, *7*, 179. [CrossRef]
10. Liu, C.; Wei, L.; Jia, X.; Gu, Y.; Guo, H.; Geng, X. Fluorinated-Polyether-Grafted Graphene-Oxide Magnetic Composite Material for Oil–Water Separation. *AppliedChem* **2023**, *3*, 400–413. [CrossRef]
11. Bayat, M.; Javanbakht, V.; Esmaili, J. Synthesis of zeolite/nickel ferrite/sodium alginate bionanocomposite via a co-precipitation technique for efficient removal of water-soluble methylene blue dye. *Int. J. Biol. Macromol.* **2018**, *116*, 607–619. [CrossRef]

12. Farhan, A.; Arshad, J.; Rashid, E.U.; Ahmad, H.; Nawaz, S.; Munawar, J.; Zdarta, J.; Jesionowski, T.; Bilal, M. Metal ferrites-based nanocomposites and nanohybrids for photocatalytic water treatment and electrocatalytic water splitting. *Chemosphere* **2023**, *310*, 136835. [[CrossRef](#)] [[PubMed](#)]
13. Benettayeb, A.; Morsli, A.; Elwakeel, K.Z.; Hamza, M.F.; Guibal, E. Recovery of Heavy Metal Ions Using Magnetic Glycine-Modified Chitosan—Application to Aqueous Solutions and Tailing Leachate. *Appl. Sci.* **2021**, *11*, 8377. [[CrossRef](#)]
14. Khoshkerdar, I.; Esmaili, H. Adsorption of Cr (III) and Cd (II) Ions using Mesoporous Cobalt-Ferrite Nanocomposite from Synthetic Wastewater. *ActaChim. Slov.* **2019**, *66*, 208–216. [[CrossRef](#)]
15. Tran, Q.A.; Tran, N.L.; Nguyen, A.D.K.; Le, T.Q.N.; Nguyen, L.T.; Nguyen, H.T.P.; Nguyen, A.T.; Nguyen, T.Q.; Le, T.K. Synthesis of Magnetic Chromium Substituted Cobalt Ferrite $\text{Co}(\text{Cr}_x\text{Fe}_{1-x})_2\text{O}_4$ Adsorbents for Phosphate Removal. *Condens. Matter. Interphases* **2022**, *24*, 306–314. [[CrossRef](#)]
16. Martinez-Vargas, S.; Valle-Ascencio, L.; Mtz-Enriquez, A.I.; Glez-Rosas, A.J.; Vázquez-Hipólito, V.; Mijangos-Ricardez, O.F.; López-Luna, J. As(III) Adsorption on Co-Precipitated Cobalt Substituted Ferrite Nanoparticles. *J. Magn. Magn. Mater.* **2021**, *539*, 168389. [[CrossRef](#)]
17. Tatarchuk, T.; Danyliuk, N.; Kotsyubynsky, V.; Shumskaya, A.; Kaniukov, E.; Ghfar, A.A.; Naushad, M.; Shyichuk, A. Eco-Friendly Synthesis of Cobalt-Zinc Ferrites Using Quince Extract for Adsorption and Catalytic Applications: An Approach Towards Environmental Remediation. *Chemosphere* **2022**, *294*, 133565. [[CrossRef](#)]
18. Mishra, S.; Sahoo, S.S.; Debnath, A.K.; Muthe, K.P.; Das, N.; Parhi, P. Cobalt Ferrite Nanoparticles Prepared by Microwave Hydrothermal Synthesis and Adsorption Efficiency for Organic dyes: Isotherms, Thermodynamics and Kinetic Studies. *Adv. Powder Technol.* **2020**, *31*, 4552–4562. [[CrossRef](#)]
19. Debnath, S.; Das, R. Strong Adsorption of CV Dye by Ni Ferrite Nanoparticles for Waste Water Purification: Fits Well the Pseudo Second Order Kinetic and Freundlich Isotherm Model. *Ceram. Int.* **2023**, *49*, 16199–16215. [[CrossRef](#)]
20. Jayalakshmi, R.; Jeyanthi, J.; Sidhaarth, K.R.A. Versatile Application of Cobalt Ferrite Nanoparticles for the Removal of Heavy Metals and Dyes from Aqueous Solution. *Environ. Nanotechnol. Monit. Manag.* **2022**, *17*, 100659. [[CrossRef](#)]
21. Tatarchuk, T.; Shyichuk, A.; Sojka, Z.; Gryboś, J.; Naushad, M.; Kotsyubynsky, V.; Kowalska, M.; Kwiatkowska-Marks, S.; Danyliuk, N. Green Synthesis, Structure, Cations Distribution and Bonding Characteristics of Superparamagnetic Cobalt-Zinc Ferrites Nanoparticles for Pb(II) Adsorption and Magnetic Hyperthermia Applications. *J. Mol. Liq.* **2021**, *328*, 115375. [[CrossRef](#)]
22. Huang, Y.; Zhang, B.; Liu, B.; Han, G.; Du, Y.; Su, S. Adsorption Behaviors of Strategic W/Mo/Re from Wastewaters by Novel Magnetic Ferrite Nanoparticles: Adsorption Mechanism Underlying Selective Separation. *J. Hazard. Mater.* **2022**, *424 Pt D*, 127675. [[CrossRef](#)]
23. Gonsalves, J.M.; Faria, L.V.; Nascimento, A.B.; Germscheidt, R.L.; Patra, S.; Hernández-Saravia, L.P.; Bonacin, J.A.; Munoz, R.A.A.; Angnes, L. Sensing performances of spinel ferrites MFe_2O_4 (M = Mg, Ni, Co, Mn, Cu and Zn) based electrochemical sensors: A review. *Anal. Chim. Acta* **2022**, *1233*, 340362. [[CrossRef](#)]
24. Slavu, L.M.; Rinaldi, R.; Di Corato, R. Application in Nanomedicine of Manganese-Zinc Ferrite Nanoparticles. *Appl. Sci.* **2021**, *11*, 11183. [[CrossRef](#)]
25. Bini, M.; Ambrosetti, M.; Spada, D. ZnFe_2O_4 , a Green and High-Capacity Anode Material for Lithium-Ion Batteries: A Review. *Appl. Sci.* **2021**, *11*, 11713. [[CrossRef](#)]
26. Tomina, E.V.; Kurkin, N.A.; Doroshenko, A.V. Synthesis of Nanoparticulate Cobalt Ferrite and Its Catalytic Properties for Fenton-Like Processes. *Inorg. Mater.* **2022**, *58*, 701–705. [[CrossRef](#)]
27. Azar, M.S.; Raygan, S.; Sheibani, S. Effect of Chemical Activation Process on Adsorption of As(V) Ion from Aqueous Solution by Mechano-Thermally Synthesized Zinc Ferrite Nanopowder. *Int. J. Miner. Metall. Mater.* **2020**, *27*, 526–537. [[CrossRef](#)]
28. Amin, A.M.M.; Rayan, D.A.; Ahmed, Y.M.Z.; El-Shall, M.S.; Abdelbasir, S.M. Zinc Ferrite Nanoparticles from Industrial Waste for Se (IV) Elimination from Wastewater. *J. Environ. Manag.* **2022**, *312*, 114956. [[CrossRef](#)] [[PubMed](#)]
29. Tang, H.; Peng, Z.H.; Wang, L.; Shang, W.; Anzulevich, A.; Rao, M.; Li, G. Facile synthesis of zinc ferrite as adsorbent from high-zinc electric arc furnace dust. *Powder Technol.* **2022**, *405*, 117479. [[CrossRef](#)]
30. Garg, J.; Chiu, M.N.; Krishnan, S.; Kumar, R.; Rifah, M.; Ahlawat, P.; Jha, N.K.; Kesari, K.K.; Ruokolainen, J.; Gupta, P.K. Emerging Trends in Zinc Ferrite Nanoparticles for Biomedical and Environmental Applications. *Appl. Biochem. Biotechnol.* **2023**, *14*, 1–36. [[CrossRef](#)] [[PubMed](#)]
31. Ajibade, P.A.; Nnadozie, E.C. Synthesis and Structural Studies of Manganese Ferrite and Zinc Ferrite Nanocomposites and Their Use as Photoadsorbents for Indigo Carmine and Methylene Blue Dyes. *ACS Omega* **2020**, *5*, 32386–32394. [[CrossRef](#)] [[PubMed](#)]
32. Qin, M.; Shuai, Q.; Wu, G.; Zheng, B.; Wang, Z.H.; Wu, H. Zinc ferrite composite material with controllable morphology and its applications. *Mater. Sci. Eng. B* **2017**, *224*, 125–138. [[CrossRef](#)]
33. Khezami, L.; Alwqyan, T.S.; Bououdina, M.; Al-Najar, B.; Shaikh, M.N.; Modwi, A.; Taha, K.K. Dependence of Phase Distribution and Magnetic Properties of Milled and Annealed $\text{ZnO} \cdot \text{Fe}_2\text{O}_3$ Nanostructures as Efficient Adsorbents of Heavy Metals. *J. Mater. Sci. Mater. Electron.* **2019**, *30*, 9683–9694. [[CrossRef](#)]
34. Naz, S.; Rasheed, T.; Raza Naqvi, S.T.; Hussain, D.; Fatima, B.; Haq, M.N.; Majeed, S.; Shafi, S.; Rizwan, K.; Ibrahim, M. Polyvinylpyrrolidone decorated manganese ferrite based cues for the efficient removal of heavy metals ions from waste water. *Phys. B Condens. Matter.* **2020**, *599*, 412559. [[CrossRef](#)]
35. Mohammed, N.A.H.; Shamma, R.N.; Elagroudy, S.; Adewuyi, A. Copper ferrite immobilized on chitosan: A suitable photocatalyst for the removal of ciprofloxacin, ampicillin and erythromycin in aqueous solution. *Catal. Commun.* **2023**, *182*, 106745. [[CrossRef](#)]

36. Guo, Y.; Guo, Y.; Tang, D.; Liu, Y.; Wang, X.; Li, P.; Wang, G. Sol-gel synthesis of new ZnFe₂O₄/Na-bentonite composites for simultaneous oxidation of RhB and reduction of Cr(VI) under visible light irradiation. *J. Alloys Compd.* **2019**, *781*, 1101–1109. [[CrossRef](#)]
37. Almahri, A. The Solid-State Synthetic Performance of Bentonite Stacked Manganese Ferrite Nanoparticles: Adsorption and Photo-Fenton Degradation of MB Dye and Antibacterial Applications. *J. Mater. Res. Technol.* **2022**, *17*, 2935–2949. [[CrossRef](#)]
38. Raghavendra, N.; Nagaswarupa, H.P.; Shashi Shekhar, T.R.; Mylarappa, M.; Surendra, B.S.; Prashantha, S.C.; Ravikumar, C.R.; Anil Kumar, M.R.; Basavaraju, N. Development of clay ferrite nanocomposite: Electrochemical, sensors and photocatalytic studies. *Appl. Surf. Sci. Adv.* **2021**, *5*, 100103. [[CrossRef](#)]
39. Das, K.C.; Das, B.; Dhar, S.S. Effective Catalytic Degradation of Organic Dyes by Nickel Supported on Hydroxyapatite-Encapsulated Cobalt Ferrite (Ni/HAP/CoFe₂O₄) Magnetic Novel Nanocomposite. *Water Air Soil Pollut.* **2020**, *231*, 43. [[CrossRef](#)]
40. Agasti, N.; Gautam, V.; Pandey, N.; Genwa, M.; Meena, P.L.; Tandon, S.; Samantaray, R. Carbon nanotube based magnetic composites for decontamination of organic chemical pollutants in water: A review. *Appl. Surf. Sci. Adv.* **2022**, *10*, 100270. [[CrossRef](#)]
41. Tong, B.; Shi, L.; Liu, X. Sol-Gel Synthesis and Photocatalytic Activity of Graphene Oxide/ZnFe₂O₄-Based Composite Photocatalysts. *Front. Mater.* **2022**, *9*, 934759. [[CrossRef](#)]
42. Li, W.; Zhang, J.; Zhu, W.; Qin, P.; Zhou, Q.; Lu, M.; Zhang, X.; Zhao, W.; Zhang, S.H.; Cai, Z. Facile preparation of reduced graphene oxide/ZnFe₂O₄ nanocomposite as magnetic sorbents for enrichment of estrogens. *Talanta* **2020**, *208*, 120440. [[CrossRef](#)] [[PubMed](#)]
43. Qureshi, I.; Khan, S.; Shifa, M.S.; Wazir, A.H. Graphene oxide-based ZnFe₂O₄ catalyst for efficient adsorption and degradation of methylene blue from water. *J. Dispers. Sci. Technol.* **2022**, *43*, 282–288. [[CrossRef](#)]
44. Rad, L.R.; Anbia, M. Zeolite-based composites for the adsorption of toxic matters from water: A review. *J. Environ. Chem. Eng.* **2021**, *9*, 106088. [[CrossRef](#)]
45. Sodha, V.; Shahabuddin, S.; Gaur, R.; Ahmad, I.; Bandyopadhyay, R.; Sridewi, N. Comprehensive Review on Zeolite-Based Nanocomposites for Treatment of Effluents from Wastewater. *Nanomaterials* **2022**, *12*, 3199. [[CrossRef](#)]
46. Rodríguez-Iznaga, I.; Shelyapina, M.G.; Petranovskii, V. Ion Exchange in Natural Clinoptilolite: Aspects Related to Its Structure and Applications. *Minerals* **2022**, *12*, 1628. [[CrossRef](#)]
47. Worasith, N.; Goodman, B.A. Clay mineral products for improving environmental quality. *Appl. Clay Sci.* **2023**, *242*, 106980. [[CrossRef](#)]
48. Inchaurredo, N.S.; Font, J. Clay, Zeolite and Oxide Minerals: Natural Catalytic Materials for the Ozonation of Organic Pollutants. *Molecules* **2022**, *27*, 2151. [[CrossRef](#)]
49. Ugwu, I.M.; Igbokwe, O.A. Chapter—Sorption of Heavy Metals on Clay Minerals and Oxides: A Review. In *Advanced Sorption Process Applications*; Edebali, S., Ed.; IntechOpen: London, UK, 2019. [[CrossRef](#)]
50. Krupskaya, V.; Novikova, L.; Tyupina, E.; Belousov, P.; Dorzhieva, O.; Zakusin, S.; Kim, K.; Roessner, F.; Badetti, E.; Brunelli, A.; et al. The influence of acid modification on the structure of montmorillonites and surface properties of bentonites. *Appl. Clay Sci.* **2019**, *172*, 1–10. [[CrossRef](#)]
51. de Gennaro, B.; Aprea, P.; Liguori, B.; Galzerano, B.; Peluso, A.; Caputo, D. Zeolite-Rich Composite Materials for Environmental Remediation: Arsenic Removal from Water. *Appl. Sci.* **2020**, *10*, 6939. [[CrossRef](#)]
52. Novikova, L.; Ayrault, C.; Fontaine, C.; Chatel, G.; Jérôme, F.; Belchinskaya, L. Effect of low frequency ultrasound on the surface properties of natural aluminosilicates. *Ultrason. Sonochem.* **2016**, *31*, 598–609. [[CrossRef](#)] [[PubMed](#)]
53. Belchinskaya, L.L.; Khodosova, N.A.; Novikova, L.A.; Anisimov, M.V.; Petukhova, G.A. Regulation of Sorption Processes in Natural Nanoporous Aluminosilicates. 3. Impact of Electromagnetic Fields on Adsorption and Desorption of Formaldehyde by Clinoptilolite. *Prot. Met. Phys. Chem. Surf.* **2017**, *53*, 793–800. [[CrossRef](#)]
54. Liu, Y.; Jiang, T.; Liu, C.H.; Huang, W.; Wang, J.; Xue, X. Effect of microwave pre-treatment on the magnetic properties of Ludwigite and its implications on magnetic separation. *Metall. Res. Technol.* **2019**, *116*, 107. [[CrossRef](#)]
55. Mañosa, J.; Rosa, J.C.; Silvello, A.; Maldonado-Alameda, A.; Chimenos, J.M. Kaolinite structural modifications induced by mechanical activation. *Appl. Clay Sci.* **2023**, *238*, 106918. [[CrossRef](#)]
56. Georgopoulos, G.; Badogiannis, E.; Tsvivilis, S.; Perraki, M. Thermally and mechanically treated Greek palygorskite clay as a pozzolanic material. *Appl. Clay Sci.* **2021**, *215*, 106306. [[CrossRef](#)]
57. Paris, E.C.; Malafatti, J.O.D.; Musetti, H.C.; Manzoli, A.; Zenatti, A.; Escote, M.T. Faujasite Zeolite Decorated with Cobalt Ferrite Nanoparticles for Improving Removal and Reuse in Pb²⁺ Ions Adsorption. *Chin. J. Chem. Eng.* **2020**, *28*, 1884–1890. [[CrossRef](#)]
58. Poggere, G.; Gasparin, A.; Barbosa, J.Z.; Melo, G.W.; Corrêa, R.S.; Motta, A.C.V. Soil contamination by copper: Sources, ecological risks, and mitigation strategies in Brazil. *J. Trace Elem. Miner.* **2023**, *4*, 100059. [[CrossRef](#)]
59. Izydorczyk, G.; Mikula, K.; Skrzypczak, D.; Moustakas, K.; Witek-Krowiak, A.; Chojnacka, K. Potential environmental pollution from copper metallurgy and methods of management. *Environ. Res.* **2021**, *197*, 111050. [[CrossRef](#)]
60. Burnase, N.; Jaiswal, S.; Barapatre, A. Metal Toxicity in Humans Associated with Their Occupational Exposures Due to Mining. In *Medical Geology in Mining*; Randive, K., Pingle, S., Agnihotri, A., Eds.; Springer Geology; Springer: Cham, Switzerland, 2022; pp. 127–186. [[CrossRef](#)]
61. Zhou, B.; Zhang, T.; Wang, F. Microbial-Based Heavy Metal Bioremediation: Toxicity and Eco-Friendly Approaches to Heavy Metal Decontamination. *Appl. Sci.* **2023**, *13*, 8439. [[CrossRef](#)]

62. Mitra, S.; Chakraborty, A.; Tareq, A.M.; Emran, T.B.; Nainu, F.; Khusro, A.; Idris, A.M.; Khandaker, M.U.; Osman, H.; Alhumaydhi, F.A.; et al. Impact of heavy metals on the environment and human health: Novel therapeutic insights to counter the toxicity. *J. King Saud. Univ.—Sci.* **2022**, *34*, 101865. [CrossRef]
63. Shabbir, Z.; Sardar, A.; Shabbir, A.; Abbas, G.; Shamshad, S.; Khalid, S.; Natasha; Murtaza, G.; Dumat, C.; Shahid, M. Copper uptake, essentiality, toxicity, detoxification and risk assessment in soil-plant environment. *Chemosphere* **2020**, *259*, 127436. [CrossRef] [PubMed]
64. Khodosova, N.; Novikova, L.; Tomina, E.; Belchinskaya, L.; Zhabin, A.; Kurkin, N.; Krupskaya, V.; Zakusina, O.; Koroleva, T.; Tyupina, E.; et al. Magnetic Nanosorbents Based on Bentonite and CoFe_2O_4 Spinel. *Minerals* **2022**, *12*, 1474. [CrossRef]
65. Chen, Z.H.; Zhang, Z.H.; Qi, J.; You, J.; Ma, J.; Chen, L. Colorimetric detection of heavy metal ions with various chromogenic materials: Strategies and applications. *J. Hazard. Mater.* **2023**, *441*, 129889. [CrossRef] [PubMed]
66. Alharthi, S.S.; Al-Saidi, H.M. Spectrophotometric Determination of Trace Concentrations of Copper in Waters Using the Chromogenic Reagent 4-Amino-3-Mercapto-6-[2-(2-Thienyl)Vinyl]-1,2,4-Triazin-5(4H)-One: Synthesis, Characterization, and Analytical Applications. *Appl. Sci.* **2020**, *10*, 3895. [CrossRef]
67. Skoog, D.A.; Holler, F.J.; Crauch, S.R. Chapter 14—Application of Ultraviolet-Visible Molecular Absorption Spectrometry. In *Principle of Instrumental Analysis*, 7th ed.; Cengage Learning: Boston, MA, USA, 2017; pp. 331–352.
68. León, G.; Hidalgo, A.M.; Martínez, A.; Guzmán, M.A.; Miguel, B. Methylparaben Adsorption onto Activated Carbon and Activated Olive Stones: Comparative Analysis of Efficiency, Equilibrium, Kinetics and Effect of Graphene-Based Nanomaterials Addition. *Appl. Sci.* **2023**, *13*, 9147. [CrossRef]
69. Sahoo, T.R.; Prelot, B. Chapter 7—Adsorption processes for the removal of contaminants from wastewater: The perspective role of nanomaterials and nanotechnology. In *Micro and Nano Technologies, Nanomaterials for the Detection and Removal of Wastewater Pollutants*; Bonelli, B., Freyria, F.S., Rossetti, I., Sethi, R., Eds.; Elsevier: Amsterdam, The Netherlands, 2020; pp. 161–222. [CrossRef]
70. Paparo, R.; Carotenuto, G. Natural Clinoptilolite Characterization by SEM. Encyclopedia. Available online: <https://encyclopedia.pub/entry/11616> (accessed on 6 July 2023).
71. Hu, J.; Lo, I.M.C.; Chen, G. Comparative study of various magnetic nanoparticles for Cr(VI) removal. *Sep. Purif. Technol.* **2007**, *56*, 249–256. [CrossRef]
72. Desalegn, Y.M.; Andoshe, M.D.; Temesgen, D.D. Composite of bentonite/ CoFe_2O_4 /hydroxyapatite for adsorption of Pb (II). *Mater. Res. Express* **2020**, *7*, 115501. [CrossRef]
73. Klekotka, U.; Wińska, E.; Zambrzycka-Szelewa, E.; Satała, D.; Kalska-Szostko, B. Heavy-metal detectors based on modified ferrite nanoparticles. *Beilstein J. Nanotechnol.* **2018**, *9*, 762–770. [CrossRef]
74. Asadi, R.; Abdollahi, H.; Gharabaghi, M.; Boroumand, Z. Effective removal of Zn (II) ions from aqueous solution by the magnetic MnFe_2O_4 and CoFe_2O_4 spinel ferrite nanoparticles with focuses on synthesis, characterization, adsorption, and desorption. *Adv. Powder Technol.* **2020**, *31*, 1480–1489. [CrossRef]
75. Dyer, A.; Hriljac, J.; Evans, N.; Stokes, I.; Rand, P.; Kellet, S.; Harjula, R.; Moller, T.; Maher, Z.; Heatlie-Branson, R.; et al. The use of columns of the zeolite clinoptilolite in the remediation of aqueous nuclear waste streams. *J. Radioanal. Nucl. Chem.* **2018**, *318*, 2473–2491. [CrossRef]
76. Sprynskyy, M.; Buszewski, B.; Terzyk, A.P.; Namieśnik, J. Study of the selection mechanism of heavy metal (Pb^{2+} , Cu^{2+} , Ni^{2+} , and Cd^{2+}) adsorption on clinoptilolite. *J. Colloid Interface Sci.* **2006**, *304*, 21–28. [CrossRef]
77. Novikova, L.A.; Bogdanov, D.S.; Belchinskaya, L.I.; Kolousek, D.; Doushova, B.; Lhotka, M.; Petukhova, G.A. Adsorption of Formaldehyde from Aqueous Solutions Using Metakaolin-Based Geopolymer Sorbents. *Prot. Met. Phys. Chem. Surf.* **2019**, *55*, 864–871. [CrossRef]
78. Debnath, K.; Pramanik, A. Heterogeneous bimetallic ZnFe_2O_4 nanopowdercatalysed facile four component reaction for the synthesis of spiro[indoline-3,2'-quinoline] derivatives from isatins in water medium. *Tetrahedron Lett.* **2015**, *56*, 1654–1660. [CrossRef]
79. Wei, L.; Yang, G.; Wang, R.; Ma, W. Selective adsorption and separation of chromium (VI) on the magnetic iron–nickel oxide from waste nickel liquid. *J. Hazard. Mater.* **2009**, *164*, 1159–1163. [CrossRef] [PubMed]
80. Liandi, A.R.; Cahyana, A.H.; Kusumah, A.J.F.; Lupitasari, A.; Alfariza, D.N.; Nuraini, R.; Sari, R.W.; Kusumasari, F.C. Recent trends of spinel ferrites (MFe_2O_4 : Mn, Co, Ni, Cu, Zn) applications as an environmentally friendly catalyst in multicomponent reactions: A review. *Case Stud. Chem. Environ. Eng.* **2023**, *7*, 100303. [CrossRef]
81. Fang, L.; Kanggen, Z.H.; Quanzhou, C.H.; Wang, A.; Chen, W. Comparative study on the synthesis of magnetic ferrite adsorbent for the removal of Cd(II) from wastewater. *Adsorpt. Sci. Technol.* **2018**, *36*, 1456–1469. [CrossRef]
82. Andrejkovičová, S.; Sudagar, A.; Rocha, J.; Patinha, C.; Hajjaji, W.; Ferreira da Silva, E.; Velosa, A.; Rocha, F. The effect of natural zeolite on microstructure, mechanical and heavy metals adsorption properties of metakaolin based geopolymers. *Appl. Clay Sci.* **2016**, *126*, 141–152. [CrossRef]
83. Thanh, D.N.; Novák, P.; Vejpravova, J.; Vu, H.N.; Lederer, J.; Munshi, T. Removal of copper and nickel from water using nanocomposite of magnetic hydroxyapatite nanorods. *J. Magn. Magn. Mater.* **2018**, *456*, 451–460. [CrossRef]
84. Sery, A.A.; El-Boraey, H.A.; Abo-Elenein, S.A.; ElKorashey, R.M. CuFe_2O_4 @ hydroxyapatite composite for the environmental remediation of some heavy metal ions: Synthesis and characterization. *Water Sci.* **2021**, *35*, 154–164. [CrossRef]

85. Manimozhi, V.; Saravanathamizhan, R.; Sivakumar, E.K.T.; Jaisankar, V. Adsorption Study of Heavy Metals Removal from Wastewater Using PVA-Nano Ferrite Composites. *Int. J. Nanosci. Nanotechnol.* **2020**, *16*, 189–200.
86. Taguba, M.A.M.; Ong, D.C.; Ensano, B.M.B.; Kan, C.-C.; Grisdanurak, N.; Yee, J.-J.; de Luna, M.D.G. Nonlinear Isotherm and Kinetic Modeling of Cu(II) and Pb(II) Uptake from Water by MnFe₂O₄/Chitosan Nanoadsorbents. *Water* **2021**, *13*, 1662. [[CrossRef](#)]
87. Iqbal, Z.; Tanweer, M.S.; Alam, M. Reduced Graphene Oxide-Modified Spinel Cobalt Ferrite Nanocomposite: Synthesis, Characterization, and Its Superior Adsorption Performance for Dyes and Heavy Metals. *ACS Omega* **2023**, *8*, 6376–6390. [[CrossRef](#)] [[PubMed](#)]
88. Alia, A.E.; Salema, W.M.; Younes, S.M.; Elabdeen, A.Z. Ferrite Nanocomposite (Rice Straw-CoFe₂O₄) as New Chemical Modified for Treatment of Heavy Metal from Waste Water. *Hydrol. Current Res.* **2018**, *10*, 311. [[CrossRef](#)]
89. Singh, R.; Jasrotia, R.; Singh, J.; Mittal, S.; Singh, H. Recyclable Magnetic Nickel Ferrite-Carboxymethyl Cellulose-Sodium Alginate Bio-Composite for Efficient Removal of Nickel Ion from water. *Res. Sq.* **2023**, preprint. [[CrossRef](#)]
90. Ramadan, R. Study the multiferroic properties of BiFeO₃/Ni_{0.1}Fe_{2.9}O₄ for heavy metal removal. *Appl. Phys. A* **2023**, *129*, 125. [[CrossRef](#)]
91. Meirelles, M.R.; Malafatti, J.O.D.; Escote, M.T.; Pinto, A.H.; Paris, E.C. Magnetic Adsorbent Based on Faujasite Zeolite Decorated with Magnesium Ferrite Nanoparticles for Metal Ion Removal. *Magnetochemistry* **2023**, *9*, 136. [[CrossRef](#)]

Disclaimer/Publisher's Note: The statements, opinions and data contained in all publications are solely those of the individual author(s) and contributor(s) and not of MDPI and/or the editor(s). MDPI and/or the editor(s) disclaim responsibility for any injury to people or property resulting from any ideas, methods, instructions or products referred to in the content.